

1 **Developing a tile drainage module for Cold Regions**  
2 **Hydrological Model: Lessons from a farm in Southern**  
3 **Ontario, Canada**

4

5 Mazda Kompanizare\*<sup>&#</sup>, Diogo Costa<sup>\*+\*</sup>, Merrin L. Macrae<sup>&</sup>, John W. Pomeroy<sup>\*</sup>, Richard M. Petrone<sup>&</sup>

6 <sup>\*</sup>Centre for Hydrology, University of Saskatchewan, Canmore and Saskatoon, Canada

7 ~~+Environment and Climate Change Canada, Saskatoon, Canada~~ University of Évora, Mediterranean Institute  
8 for Agriculture, Environment and Development, Portugal

9 <sup>&</sup>University of Waterloo, Waterloo, Canada

10 <sup>#</sup>Corresponding author: kompanizare.mazda@usask.ca

11

12 **Abstract**

13 Systematic tile drainage is used extensively in agricultural lands to remove excess water and  
14 improve crop growth; however, tiles can also transfer nutrients from farmlands to downstream  
15 surface water bodies, leading to water quality problems. ~~Thus, t~~There is a need to simulate the  
16 hydrological ~~behavior~~behaviour of tile drains to understand the impacts of climate or land  
17 management change on agricultural runoff. The Cold Regions Hydrological Model (CRHM) is a  
18 physically based, modular modeling system ~~that enables creating comprehensive models~~  
19 appropriate developed for cold regions. ~~by including a full suite of winter, spring, and summer~~  
20 season processes and coupling these together via mass and energy balances. ~~Here, a~~A new tile  
21 drainage module ~~was is~~ developed for CRHM. ~~to account for this process in tile drained~~  
22 landscapes that are increasingly common in cultivated basins of the Great Lakes and northern

23 ~~Prairies regions of North America.~~ A ~~robust~~ multi-variable, multi-criteria model performance  
24 ~~(with NSE>0.29, RSR<0.84 and PBias <20 for tile flow and water table)~~ evaluation strategy was  
25 deployed to examine ~~the ability~~the ability of the module ~~with CRHM~~ to capture tile discharge  
26 under both winter and summer conditions ~~(NSE>0.29, RSR<0.84 and PBias <20 for tile flow and~~  
27 ~~water table simulations).~~ ~~However~~Initially, the module effectiveness of the model for accurate  
28 ~~prediction of observed tile flow rates was was not very high simulations done run~~ at a 15-min  
29 ~~interval did not unsatisfactorily~~ represent tile discharge; however, ~~y,~~ with the R results  
30 ~~showed~~showing that the soil moisture is was largely regulated by tile flow and lateral flow from  
31 adjacent fields. ~~However, the model simulations~~ improved when the time step was  
32 ~~smoothed refined to, with hourly but also time steps, greatly improved with the explicit~~  
33 ~~representation of~~ ~~The after the explicit representation of~~ capillary rise for moisture interactions  
34 between the rooting zone and groundwater ~~was explicitly represented~~ ~~greatly improved model~~  
35 ~~simulations,~~ ~~demonstrating~~ ~~demonstrating its the~~ significance of capillary rise in the hydrology  
36 of tile drains in loam soils. ~~Soil W water~~ Soil water level (elevation head) histogram patterns  
37 ~~revealed a bimodal behavior behaviour~~ that depended on the positioning of the capillary fringe  
38 ~~relative to the tile.~~ ~~A novel~~ Novel aspects of this module ~~is include~~ the shorter time step relative  
39 ~~to some existing models, which may enable future water quality modules to be added, and~~ the  
40 use of field capacity and its corresponding pressure head to provide ~~an~~ estimates of drainable  
41 water and the thickness of the capillary fringe, rather using than ~~a~~ detailed soil retention curves  
42 that may not always be available. An additional novel aspect of our results is the demonstration  
43 that flows in some tile drain systems can be better represented and simulated when related to  
44 shallow groundwater dynamics. ~~Understanding the bimodal nature of soil water levels provided~~  
45 ~~better insights~~ into the significance of dynamic water exchange between soil layers below drains

46 ~~to improve tile drainage representation in models. Our results also showed that in our study site~~  
47 ~~the tile drain flows is could be better more explained and related to groundwater dynamics and~~  
48 ~~appearancinteractions with e in adjacent fields.~~

49

50 Keywords: tile drainage, cold regions, hydrological model, capillary fringe, drainable water,  
51 water level fluctuations

52

53

## 54 **1. Introduction**

55

56 Harmful algal blooms and eutrophication in large freshwater lakes surrounded by agricultural  
57 lands are major environmental challenges in Canada and globally. The transport of nutrients,  
58 particularly phosphorus, in runoff from agricultural fields into rivers, ponds and eventually lakes  
59 is an important contributor to the increased frequency of algal blooms being experienced in  
60 North America and elsewhere (Sharpley et al., 1995; Correll, 1998; Filippelli, 2002; Ruttenberg,  
61 2005; Schindler, 2006; Quinton et al., 2010; [Costa et al., 2022](#)). Nutrient transport from  
62 agricultural fields can occur via both surface runoff and tile drainage (Radcliffe et al., 2015), and  
63 recent increases in the frequency and magnitude of algal blooms in Lake Erie in North America  
64 have been attributed to tile drainage (King et al., 2015; Jarvie et al., 2017). Tile drain systems  
65 reduce the retention time of soil water, lessening waterlogging in fields and improving both crop  
66 growth and field trafficability for farmers (Cordeiro and Ranjan, 2012; Kokulan et al., 2019a).  
67 However, they are also important pathways for dissolved and particulate nutrients (Kladivko et  
68 al., 1999; Tomer et al., 2015). It has been estimated that 14% of farmlands in Canada (ICID,

69 2018) and 45% of fields in Southern Ontario, Canada (ICID, 2018; Kokulan, 2019) are drained  
70 by tile systems. In Alberta, tile drains have also been used to address salinity issues (Broughton  
71 and Jutras, 2013). Given their importance in hydrological budgets and biogeochemical transport,  
72 there is a need to understand the controlling mechanisms of water and nutrient export from tile  
73 systems as an integral part of the broader, modified hydrological system. The ability to integrate  
74 a dynamic quantification of tile drainage from fields in hydrological models can help understand  
75 the relative importance of this human-induced process as it interplays with an array of other  
76 phenomena, including energy and physical mass balance hydrological processes, climate change,  
77 and the impacts of modified land management practices on runoff and nutrient export.

78         There are several models that can represent tile drainage at the small basin scale, such as  
79 HYPE (Lindstrom et al., 2010; Arheimer et al., 2015), DRAINMOD (Skaggs, 1978, 1980a;  
80 Skaggs et al., 2012), MIKE SHE (Refsgaard and Storm, 1995) and SWAT (Arnold et al., 1998;  
81 Koch et al., 2013; Du et al., 2005; Du et al., 2006; Green et al., 2006; Kiesel et al., 2010). These  
82 models include conceptual components for many key hydrological processes, but research shows  
83 that they have been primarily designed and tested for temperate regions (Costa et al., 2020a). In  
84 Canada and other cold regions, some unique hydrological processes such as frozen soil,  
85 snowmelt, rain on snow, and runoff over and infiltration into frozen or partially-frozen soils may  
86 be very important (Rahman et al., 2014; Cordeiro et al., 2017; Pomeroy et al., 1998, 2007; Fang  
87 et al., 2010, 2013). Many hydrological processes, such as the sublimation of snow, energy  
88 balance snowmelt, and infiltration into frozen soils, are strongly affected by temperature and the  
89 phase changes of water, which make many existing models developed for warm regions less  
90 appropriate for regions with cold seasons (Pomeroy et al., 2007; Pomeroy et al., 2013; Pomeroy

91 et al., 2016; Fang et al., 2010, 2013). Even for temperate regions, the representation of cold  
92 season processes is often underrepresented in models (Costa et al., 2020a).

93         Since the use of tile drainage is becoming popular in many cold regions, it has become  
94 important to integrate such human-induced process in specialized hydrological modelling tools  
95 for these regions, such as the Cold Regions Hydrological Modelling platform (CRHM, Pomeroy  
96 et al., 2007; 2013; 2022). CRHM was initially developed in 1998 to assemble and explore the  
97 hydrological understanding developed from a series of research basins spanning Canada and  
98 elsewhere into a flexible, modular, object-oriented, multiphysics platform for simulating  
99 hydrological processes and basin response in cold regions (Pomeroy et al., 2007; 2022). The  
100 modular CRHM platform allows for multiple representations of forcing data interpolation and  
101 extrapolation, hydrological model spatial and physical process structure and parameter values.  
102 Many existing models typically operate at default daily or monthly time intervals, which is  
103 inadequate for the prediction of many short-duration “flashy” hydraulic responses often observed  
104 in tiles (Puer et al., 2020; Vivekananthan, 2019; Vivekananthan et al., 2019; Lam et al., 2016a,  
105 2016b; Macrae et al., 2019). Indeed, the ability to simulate shorter time intervals (e.g., hourly)  
106 facilitates the ability to capture both the rising and falling limbs of tile flow hydrographs, as well  
107 as the magnitude of peak flows, both of which are important to tile drain chemistry and export  
108 (Rozemeijer et al., 2016; Williams et al., 2015, 2016; Macrae et al., 2019).

109         Hydrological process models such as DRAINMOD, MIKE SHE and SWAT use a  
110 combination of empirical and physically —-based formulations for the simulation of tile flow  
111 derived by Hooghoudt (1940), Kirkham (1957), van Schilfgaarde (1974), Bouwer and van  
112 Schilfgaarde (1963) and Skaggs et al., (1978). Such formulations contemplate both cases where  
113 the soil-water level-table is below and above the ground surface (Kirkham, 1957). In contrast,

114 simulations of tile drainage in other models such as HYPE use empirically-derived recession  
115 curves (Eckersten et al., 1994) to simulate tile flow and water levels/soil hydrological storage  
116 (typically represented as water table position). In cases where there is a need for more focus on  
117 soil matrix hydrology and less need for understanding the hydrological processes at the  
118 catchment scale and the relative contribution of tiles (and its interplay) ~~with other catchment~~  
119 ~~scale mass balance hydrological processes~~, -modellers tend to use specialised porous-media  
120 PDE-based (partial differential equation-based) numerical models such as HYDRUS (Simunek et  
121 al., 2011) and MACRO (Larsbo and Jarvis, 2003).

122         The amount of water -transported by tiles depends on soil moisture dynamics and the  
123 positioning of the water table, which are in turn affected by many factors, including soil type,  
124 surface topography and morphology, as well as the local climate and the hydrological  
125 characteristics of the field (Frey et al. 2016; Klaiber et al., 2020; Coelho et al., 2012; King et al.,  
126 2015). Thus, to provide reliable estimations of water outflow/loss -from farmland via surface  
127 runoff and tile flow, models must be able to predict soil moisture storage and the soil-water level  
128 table position accurately (Brockley, 1976; Rozemeijer et al., 2016; Javani-Jouni et al., 2018).  
129 Many studies have shown that in some soil types, including silty loam and clay loam soils, the  
130 drainable water is less than expected based on the effective porosity (*e.g.*, Skeggs et al., 1978;  
131 Raats and Gardner, 1974). Raats and Gardner (1974) have argued that the calculation of  
132 drainable porosity requires knowledge of the soil-water level table position and the distribution  
133 of soil moisture above the water level table. Skeggs-Skaggs et al. (1978) added that the  
134 calculation of drainable porosity should take into account “the unsaturated zone drained to  
135 equilibrium with the water table”. However, because the soil column is often composed of  
136 different soil layers with varying physical characteristics, drainable porosity varies with

137 evapotranspiration rate, soil water dynamics and the depth of saturated water ~~level~~ depth  
138 (Logsdon et al., 2010; Moriasi et al., 2013). In a sandy loam soil, Lam et al. (2016a, 2016b)  
139 demonstrated that tile drainage was not initiated until soils ~~were~~ was at or above field capacity.  
140 Williams et al. (2019) observed in the American Midwest that tile drainage was not initiated until  
141 the field storage capacity had been exceeded. It has also been shown that despite the presence of  
142 tile drains, the soil above the tile may not always drain all gravitational water appreciably  
143 considerably into the tile following a rainfall/snowmelt event and the soil may remain at or  
144 above field capacity (Skaggs et al., 1978; Lam et al., 2016a). Therefore, the soil drainable water  
145 content may be considerably smaller than the storage capacity. This is related to matric potential  
146 within the vadose zone, which is driven by the soil characteristics but can also be due to the  
147 development of a capillary fringe that reduces the rate of vertical percolation through the  
148 unsaturated zone, reducing tile flow (Youngs, 2012). Despite this evidence, some saturated flow  
149 models that simulate tile flow overlook the effect of capillary rise and over-estimate the soil  
150 drainable water. Other models that represent unsaturated flow (i.e., HYDRUS 3D, Simunek et  
151 al., 2011) using Richard's Equation (Richards, 1931) capture the effect of capillary rise and  
152 saturation-pressure variation within the soil profile and assess the soil drainable water more  
153 accurately. Although the effect of capillary rise is considered in DRAINMOD through the  
154 concept of drainable porosity (~~that is~~ represented as a "water yield") (Skaggs, 1980b), and is  
155 calculated for layered soil profiles (Badr, 1978), it requires detailed information surrounding the  
156 soil water characteristic curve (Skaggs, 1980b). ~~It~~ Although it is indeed optimal to use soil-  
157 specific water characteristic curves, ~~;~~ however, Twarakawi et al. (2009) found that it was  
158 possible to employ average representative values from the soil water characteristic curve to

159 represent soil drainable water where a soil-specific curve ~~is~~was not available. They found in  
160 this case; although that the model performance was reduced.

161 In this study, a new tile drainage module was developed and incorporated within the  
162 physically based, modular Cold Regions Hydrological Modelling (CRHM) platform (Pomeroy et  
163 al., 2022) to enable hydrological simulations in tile-drained farm fields in cold agricultural  
164 regions. As a first iteration, the new module was developed for a field with sloping ground and  
165 loam soil with imperfect drainage. Such landscapes are common in the Great Lakes Region (e.g.  
166 Michigan and Vermont, USA and Ontario, Canada) and tile drainage in such landscapes has not  
167 been as widely studied as it has been in clay-dominated soil. In this module, considerations were  
168 explicitly included for the effects of capillary rise and annual groundwater water table  
169 fluctuations on drainable soil water storage. The use of field capacity and pressure  
170 groundwater/soil water elevation head (Twarakawi et al., 2009) to modulate soil drainable water  
171 across the soil profile, including the capillary fringe region, is an innovative aspect of the model  
172 that has been demonstrated to ~~negate~~circumvent the need for water characteristic curves. The  
173 development of this physically -based module provides insight into hydrological processes in tile  
174 drainage from sloping landscapes with imperfect drainage, which are increasingly being  
175 artificially drained.

176

## 177 **2. Materials and Methods**

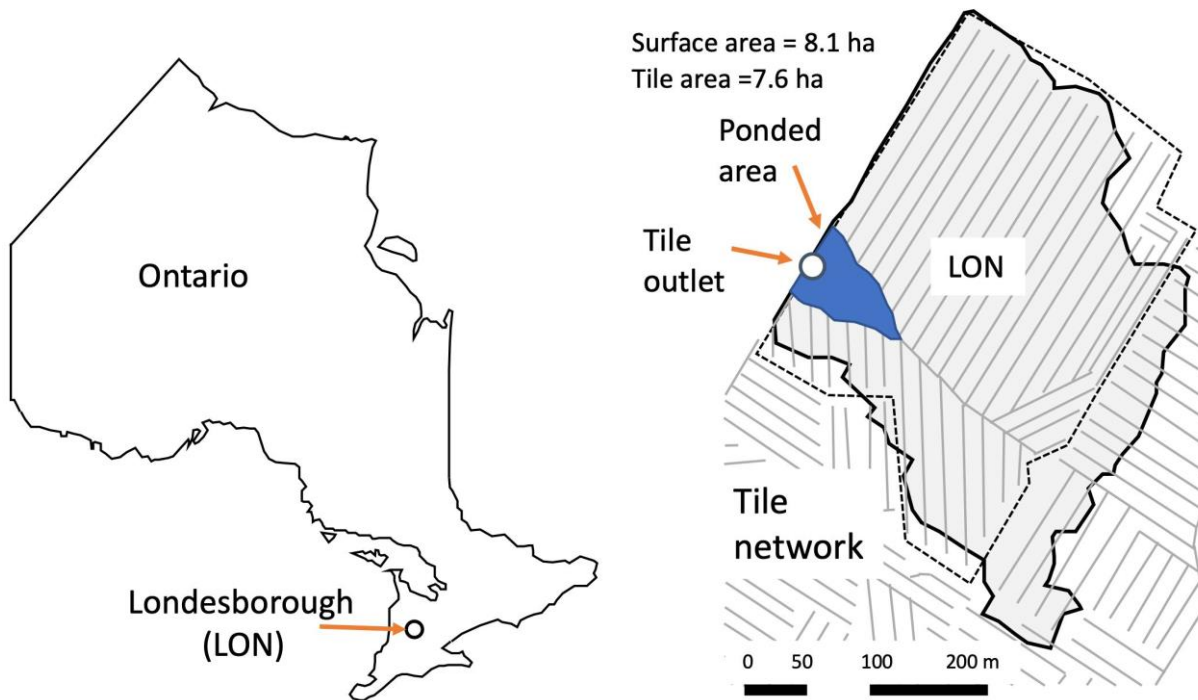
### 178 *2.1 Study area*

179 The study site is a ~10 ha farm field located near Londesborough, Ontario at LON (UTM 17T  
180 466689m E, 4832203m N), shown as LON in Ontario (Fig. 1a). Mean annual precipitation  
181 recorded in this region is 1247 mm (ECCC, 2020). Mean air temperature is 7.2 °C, with annual



182 maxima in July (25.9 °C) and minima in January (-10.2 °C), (ECCC, 2020). Soil texture has been  
183 identified as Perth clay loam (Gr. Br. Luvisolic), with a slope between 0.2 and 3.5%. The field is  
184 systematically drained with a tile depth of 0.9 m and a spacing of 14 m (laterals). The tile  
185 network collects infiltrated water from about 75% of the field (~ 7.6 ha), ~~but~~ but may also  
186 receive lateral as well as shallow groundwater flows from neighbouring areas/fields. Water yields  
187 from the tile drain laterals (10 cm diameter) are, which is discharged via a common tile outlet  
188 (main, 15 cm diameter) below ground. Surface runoff from the field is directed toward a  
189 common outlet on the surface using plywood berms installed along the field edge (see van  
190 Esbroeck et al., 2016). The tile and surface runoff outlets do not join into a common outlet and  
191 are fully separated from one another, even during surface ponding events. The field is a corn-  
192 soy-winter wheat rotation with cover crops and rotational conservation till (shallow vertical  
193 tillage every three years). Additional details related to farming practices are provided in Plach et  
194 al. (2019), ~~and~~ soil characteristics are provided in Plach et al. (2018a) and Plach et al. (2018b)  
195 and equipment and monitoring are provided in van Esbroeck et al., (2016). The outlets ~~of~~ for  
196 both the surface and tile flows are located at the edge of the field and drain into an adjacent field  
197 (Fig. 1b). Water tends to accumulate in a topographic low in the field, in front of the field outlet  
198 during snowmelt or high-intensity rainfall events, presumably due to either surface runoff or  
199 return flow (see ponded area, Fig. 1b). However, surface water or elevated soil moisture  
200 conditions are not observed in this topographic low during smaller events or dry periods of the  
201 year, suggesting that this saturated ponding is not in a perennial groundwater discharge zone.  
202 Although surface ponding is observed in the topographic depression within the field, water  
203 discharges freely at the opposite end of the culvert, facilitating the measurement of flow. The  
204 accumulated water in ponded area, based on our field observations, is originated from snowmelt

205 and surface runoff rather than groundwater discharge. It should also be mentioned that the tile  
206 drain edge of field outlet pipe is always separated and isolated from the surface flow outlet, even  
207 during surface ponding events. This zone coincides with the tile drain main pipe and is not a zone  
208 of groundwater discharge.  
209



210  
211 a)  
212 b) Figure 1. (a) Location of the study area in South of Ontario and the (b) Londesborough (LON) farm with its tile network.  
213  
214

## 215 2.2 CRHM: The modelling platform

216 The modular CRHM platform includes options for empirical and physically based calculations of  
217 precipitation phase, snow redistribution by wind, snow interception, sublimation, sub-canopy  
218 radiation, snowmelt, infiltration into frozen and unfrozen soils, hillslope water movement, actual

219 evapotranspiration, wetland fill and spill, soil water movement, groundwater flow and  
220 streamflow (Pomeroy et al., 2007; 2022). Where appropriate, it calculates runoff from rainfall  
221 and snowmelt as generated by infiltration excess and/or saturated overland flow, flow over  
222 partially frozen soils, detention flow, shallow subsurface flow, preferential flow through  
223 macropores and groundwater flow. Water quality can also be simulated (Costa et al., 2021).

224 Modules of a CRHM model can be customized to basin setup, such as delineating and  
225 discretizing the basin, conditioning observations for extrapolation and interpolation in the basin,  
226 or are process-support algorithms such as for estimating longwave radiation, complex terrain  
227 wind flow, or albedo dynamics, but most modules commonly address hydrological processes  
228 such as evapotranspiration, infiltration, snowmelt, and streamflow discharge. CRHM discretizes  
229 basins into hydrological response units (HRU) for mass and energy balance calculations, each  
230 with unique process representations, parameters, and position along flow pathways in  
231 the basin. HRU are connected by blowing snow, surface, subsurface and groundwater flow and  
232 together generate streamflow which is routed to the basin outlet. The size of TDM HRUs is  
233 flexible and can be as small as the size of a single tile pipe (e.g.e.g., 1 m) times the pipe spacing  
234 (which was 14 m in our case study region), and as large as entire tile networks within a given  
235 farm or study area. CRHM does not require a stream within a modelled basin. The feature allows  
236 CRHM to model the hydrology of cold regions dominated by storage and episodic runoff, such  
237 as agricultural fields.

238 Although CRHM has the capabilities to represent many hydrological and  
239 thermodynamic processes, not all processes need to be represented in all situations.  
240 The modular design of the CRHM platform enables the user to activate or inactive specific  
241 processes to optimize the model for a particular situation. This is a modelling approach that

242 enables testing different modelling hypotheses and has been pioneered by CRHM and other  
243 models, which has inspired a range of hydrological (e.g., SUMMA, Clark et al., 2015a, 2015b),  
244 hydrodynamic (e.g., mizuRoute, Mizukami et al., 2015) and biogeochemical (e.g., OpenWQ,  
245 Costa et al., 2023a, 2023b) modelling tools. -For example, in the current study, blowing snow  
246 was not employed in CRHM as it does not appear to be significant at the study site (periodic  
247 snow surveys showed relatively uniform snow cover). Preferential flow into tile drains was not  
248 developed for the current simulation as although it is a key process in heavy clay soil, as it does  
249 not appear to be a significant driver of preferential flow into tile drains in coarse textured soil  
250 (Pluer et al., 2020; Macrae et al., 2019). Freeze-thaw processes in soil were also not employed  
251 here as there is very little seasonal soil frost in the temperate Great Lakes region due to the  
252 persistent snow cover, and where soil frost occurs, it is restricted to brief periods and shallow  
253 depths (above 10 cm depth) (Macrae unpublished data).

254

### 255 2.3 *Observations and input data for the model*

256 Tile flow, ~~soil-water level-table position~~ (water table ~~position~~elevation head) and surface flow  
257 were measured at the site between Oct. 2011 and Sept. 2018 at 15-minute intervals. It was not  
258 possible to install more than one measuring station for water table position and soil moisture at  
259 the site due to farming activity; ~~consequently, so-water table position~~water table elevation head  
260 and soil moisture were measured at the ~~field edge~~, approximately ~~at the~~ midpoint of the field at  
261 the edge-of-field. ~~Both tile flow rates and surface runoff~~ Tile flow rates were determined using  
262 simultaneous measurements of flow velocity and water ~~level~~depths in each of the ~~tile main~~  
263 pipes at the ~~edge~~edge-of-the field using Hach Flo-tote sensors and an FL900 data logger (Onset  
264 Ltd.) (Table A1, Appendix A). Continuous measurements of velocity were included due to the

265 potential for impeded drainage under very wet conditions or caused by the accumulation of snow  
266 and ice around the surface culvert in winter. A, with an additional barometrically-corrected  
267 pressure transducer (U20, Onset Ltd.) (Table A1) was also used for periods when the flow  
268 sensors did not function using a rating curve developed from the depth-velocity sensors. Surface  
269 runoff naturally exits the field at one location. However, to facilitate its measurement, the edges  
270 of the field were equipped with berms (1/2 plywood sheets, installed vertically above and below  
271 the ground), directing surface runoff through a culvert (45 cm diameter). Surface runoff through  
272 the culvert was also measured using a Hach Flo tote sensor and FL900 logger. The soil-water  
273 level table position in the field was measured at the edge of the field, located midway between  
274 the topographic high and low points of the field, was measured using a baro-corrected pressure  
275 transducer (U20, Onset Ltd.).

276 Air temperature, wind speed, air relative humidity, incoming solar irradiance and rainfall  
277 were also measured at the site at 15-minute intervals and used to force the model. Variable  
278 names and their symbols in CRHM are listed in Appendix B. The air temperature, wind speed  
279 and incoming solar radiance measurements were collected 1 m above ground using a  
280 Temperature Smart Sensor S-THB-M002, Wind Smart Sensor Set S-WSET-M002 and a Solar  
281 Radiation Sensor (Table A1). Rainfall and relative humidity were measured via a tipping bucket  
282 rain gauge (Table A1) and ~~aan~~ RH Smart Sensor (Table A1). These observations were  
283 continuously recorded throughout the study period, ~~with the exception of~~ except for brief periods  
284 of instrument failure and maintenance, when data from nearby stations (Table T1,  
285 Supplementary Material) was substituted using the double mass analysis method (Searcy and  
286 Hardison, 1960).

287 Although rainfall was recorded continuously at the field site, snowfall data was not.  
288 Snowfall data was obtained from nearby stations (Wroxeter-Davis and Wroxeter, Environment  
289 Canada, 2021), located 31.7 km from the field site. Periodic snow surveys done at the site  
290 [throughout the study period](#) found that data from the nearby stations was a close approximation  
291 of snow at the field site ([Plach et al., 2019](#)). Hourly ~~precipitation-snowfall data-observations~~ from  
292 Wroxeter-Geoneor were used for the period between 2015 and 2018, whereas daily ~~data-data~~  
293 from the ~~Wroxeter station and the daily pattern of snowfall from~~ Wroxeter-Geoneor were  
294 ~~combined for the period between~~ used for the 2011 ~~and to~~ 2014 ~~period, reconstructed to hourly~~  
295 ~~for reconstruction of the missing hourly~~ snowfall time series based on the method presented by  
296 Waichler and Wigmosta (2003).

297

#### 298 2.4 Development of the new tile module

299 A Tile Drainage Module (TDM) was developed within CRHM with the goal of adding the ability  
300 to simulate tile flow and the resulting ~~soil-water levels~~ saturated storages ([soil-water tablewater](#)  
301 [table](#)) at an hourly time scale. CRHM was forced with hourly precipitation, air temperature, solar  
302 radiation, wind speed and relative humidity to calculate hydrological states and fluxes in HRUs  
303 and the basin. The model requires parameterizations that specify the hydraulic and hydrological  
304 properties of the soil, including its thickness, saturated hydraulic conductivity (K), and surface  
305 cover. CRHM calculates water storage and fluxes between HRUs, as well as vertical fluxes  
306 amongst different hydrological compartments (within each HRU) that include snow,  
307 depressional storage, different soil layers, and groundwater.

308 ~~Based on~~ Using the simulation of soil moisture performed by the original CRHM “Soil”  
309 module, TDM calculates the dynamic tile flow rate that, in turn, feeds back to soil moisture at

310 each time step. The presence of a capillary fringe (sometimes referred to as the tension-saturated  
311 zone within the soil profile) and its effects are considered by limiting the amount of drainable  
312 soil water. TDM uses ~~specific~~ site-specific information ~~about~~ regarding the tile network, such as  
313 ~~the~~ tile depth, diameter and spacing. Information regarding site-specific details regarding tile  
314 depth, diameter and spacing may be obtained directly from landowners or can be estimated based  
315 on standard design and installation guidelines for the region. ~~This information was used,~~ to set  
316 up the model together with ~~a parameterisation~~ parameterization ~~that~~ to translates the hydrological  
317 effects of the soil capillary fringe (CF), if present, ~~into~~ through two state variables, CF thickness  
318 and CF drainable water (discussed in Section 2.5). These two state variables are used to limit the  
319 fraction of the soil moisture that can freely drain to the tiles.

320

#### 321 2.4.1 Soil moisture and water ~~level~~ table position

322 The TDM uses the water quality soil module or soil module ( $WQ_{soil}$  or *Soil*), which divides the  
323 soil column into two layers: a recharge layer where evapotranspiration and root uptake generally  
324 take place and a deeper layer that connects to the groundwater system. Since CRHM's state  
325 variable for soil moisture is soil water storage volume (Fig. 2a), the model results were converted  
326 into water level elevation above the semi-permeable layer (Table B1, Appendix B; see Fig. 2b  
327 for comparison with ~~soil~~ water level table observations) by dividing volumetric soil moisture  
328 content (Table B1) by soil porosity (Table B1) for the cases with no capillary fringe above the  
329 ~~soil~~ water level table. Additional steps were taken for periods when a capillary fringe developed  
330 (discussed below).

331

#### 332 2.4.2 Capillary fringe and drainable water

333 Soil moisture in the capillary fringe is equal to the field capacity ( $\theta_{fc}$ ) (Bleam, 2017, Sect. 2.4).

334 Therefore, while the positioning of the capillary fringe responds dynamically to the matric

335 potential, the saturation profile within the capillary fringe remains constant, as well as its

336 thickness because it only depends on the pressure head (capillary forces) that are related to the

337 grain size distribution and field capacity ( $h_{fc}$ ) as introduced by Twarakawi et al. (2009).

338 Therefore, the drainable water in the capillary fringe becomes the difference between saturation

339 ( $\theta_s$ ), computed dynamically in CRHM, and  $\theta_{fc}$ , which corresponds to the water held by capillary

340 forces at field capacity (Fig. 2). Accordingly, Fig. 2 shows the schematic soil characteristic curve

341 for the three water level conditions contemplated in the model.

342 1. *Condition 1* is when the matric head is at the surface and the soil is completely saturated;

343 2. *Condition 2* is when the matric head drops but the upper boundary of the capillary fringe

344 is at the soil surface; and

345 3. *Condition 3* is when [the soil-water level table](#) drops further and the upper boundary of

346 the capillary fringe drops beneath the surface.

347 In essence, the soil is completely saturated ( $\theta_s$ ) in *Condition 1*. Between *Conditions 1* and 2, the

348 capillary fringe occupies the entire soil column above the water level; thus, it can only release

349 the volume of water corresponding to  $\theta_s - \theta_{fc}$  or  $\varphi_c$  (dimensionless). Between *Conditions 2* and 3,

350 two layers with distinct hydraulic characteristics develop: (1) the top one at  $\theta_{wp}$  that releases

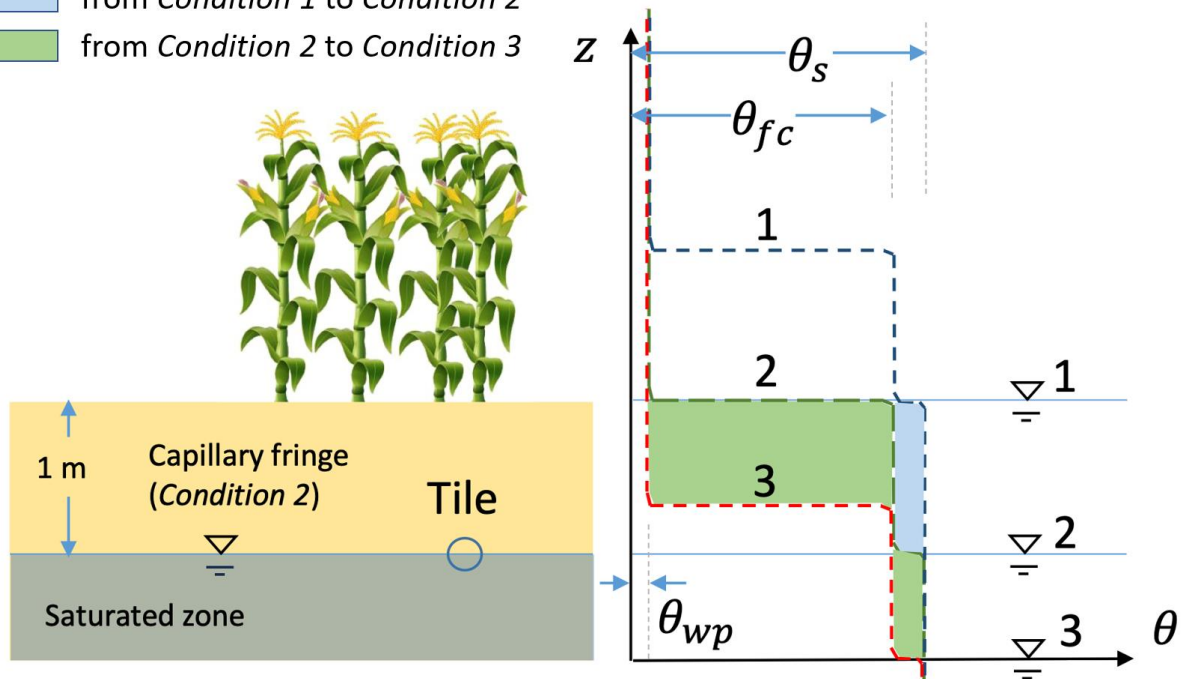
351 water up to  $\theta_{fc} - \theta_{wp}$ , and (2) the lower one that corresponds to the capillary fringe and can

352 release up to the volume of water corresponding to  $\theta_s - \theta_{fc}$  or  $\varphi_c$ .



Drained water when the water table position is changed:

- from *Condition 1* to *Condition 2*
- from *Condition 2* to *Condition 3*



353

354 Figure 2. Schematic representation of the capillary fringe above the soil-water level table assuming a 1-m thickness (for  
 355 demonstration purposes). The soil characteristic curves are shown for the three water level conditions considered: water level at  
 356 the (1) surface, (2) intermediate depth, and (3) deeper depth. Two transitional drops can be seen in the characteristic curves, one  
 357 from saturation ( $\theta_s$ ) to field capacity ( $\theta_{fc}$ ) (between *Conditions 1* and *2*) and one from field capacity to wilting point ( $\theta_{wp}$ )  
 358 (between *Conditions 2* and *3*). The colored areas (green and blue) of the right panel correspond to the amount of water  
 359 that can be released between *Conditions 1* and *2* (blue) and between *Conditions 2* and *3* (green).

360

361

### 362 2.4.3 Tile flow calculation

363 A modified version of the Hooghoudt equation was used to calculate tile flow (Smedema et al.,  
 364 2004), which presumes no surface ponding, an assumption that generally holds at the study site  
 365 (Eq. 1), where water ponds only during very wet periods and on a small portion of the study site  
 366 (see Fig. 1b). Hooghoudt's equation (Hooghoudt, 1940) is a steady state, physically based

367 equation for saturated flow toward the tile drain. Flow estimates are provided based on the  
 368 hydraulic conductivity of the soil and matric potential. It allows different saturated hydraulic  
 369 conductivities for the layers above (AL) and below (BL) the tile (Fig. S1). In the particular case  
 370 of the case study site, soil surveys have reported almost the same soil type (Loam) down to the  
 371 depth of 90 cm (*e.g.e.g.*, Van Esbroeck et al., 2016; Plach et al., 2018b), which was  
 372 parameterized in the model set up as,

$$q = \frac{8 \times K_2 \times d \times h}{L^2} + \frac{4 \times K_1 \times h^2}{L^2}, \quad (1)$$

376 where  $K_1$  and  $K_2$  are respectively the saturated hydraulic conductivity in the upper and lower  
 377 layers in  $\text{mm h}^{-1}$ ;  $L$  is the tile spacing in mm;  $h$  is the soil-water level-table elevation above the  
 378 tile in mm,  $d$  is the lower layer thickness in mm (Fig. S1), and  $q$  is the predicted tile flow in  $\text{mm}$   
 379  $\text{h}^{-1}$ . The only variable that is dynamically updated by CRHM is  $h$ . Equation (1) is used to  
 380 estimate the tile flow.

#### 382 2.4.4 Calculation of the effect of tile flow on soil moisture and water levels

383 The simulated tile flows (see Sect. 2.3.3) are subtracted from the soil moisture. To calculate a  
 384 saturated storage-water level (soil-water-tablewater table or groundwater elevation head level)  
 385 from soil moisture calculated by the model, a threshold soil moisture content ( $sm_t$ ) is defined,  
 386 which consists of drainable water in the soil when the upper boundary of the capillary fringe is at  
 387 the surface (*Condition 2*, Fig. 2) and ean-bewas calculated as:

$$389 \quad sm_t = sm_{max} - (C_t \times \varphi_c) , \quad (2)$$

390

391 where  $sm_{max}$  is the maximum soil moisture and  $C_t$  is the capillary fringe thickness in mm.

392 However, since the hydrological conditions of the soil are markedly different between the two

393 transitional situations described in Sect. 2.3.2 and Fig. 2 (*Condition 1* to 2 and *Condition 2* to 3),

394 a step function ~~had to be considered~~ was deployed for determination of the matric potential:

395

396 
$$SWLT = \begin{cases} \frac{sm_t - (C_t \times ((\varphi_s - \varphi_c) + \theta_{wp}))}{\varphi_s + \theta_{wp}} + \frac{sm - sm_t}{\varphi_c} & , \text{if between Conditions 1 and 2} \\ \frac{sm_{max}}{\varphi_s + \theta_{wp}} - \left( \left( \frac{sm_t - sm}{\varphi_s} \right) + C_t \right) & , \text{if between Conditions 2 and 3} \end{cases} \quad (3)$$

397

398 where  $SWLT$  is soil-water level-table elevation (or soil saturated storage, SSS) in mm from the

399 bottom of the soil, and  $sm$  is soil moisture (both saturated and unsaturated storage) in the given

400 time step in mm. Equation (3) is determined based on soil moisture curves in Fig. 2 and water

401 level *Conditions 1-3* discussed in Sect. 2.3.2. In Fig. 2, the first and second parts of Eq. (3),

402 which refer to *Conditions 1* to 2 and 2 to 3, respectively, correspond to the volumes of soil water

403 highlighted in “blue” and “green.”

404

#### 405 2.4.5 Lower semi-permeable soil layer and periodicity in annual groundwater levels

406 This model application focused on the study site field without including other adjacent areas.

407 This was possible because years of field monitoring at this site have demonstrated that there is no

408 observable surface flow into the site from adjacent farms. The tile network is restricted to the

409 field and is not connected to tile drains or surface inlets in adjacent fields. However, field soil

410 water level-table observations show evidence of annual groundwater level periodicity/fluctuation

411 (Rust et al., 2019) that are sinusoidal in nature and cannot be neglected. Some studies predict the  
 412 annual groundwater oscillations or the annual responses of groundwater to precipitation by using  
 413 sine and cosine functions (De Ridder et al., 1974; Malzone et al., 2016; Qi et al., 2018). De  
 414 Ridder et al. (1974) studied the design of the drainage systems and described the seasonal  
 415 groundwater fluctuations observed in wells using sinusoidal curves. Malzone et al. (2016) used a  
 416 sine function to predict annual groundwater fluctuations in the hyporheic zone. Qi et al. (2018)  
 417 and Rust et al (2019) used a cross-wavelet transform, consisting of the superposition of sine and  
 418 cosine curves, to predict shallow groundwater response to precipitation at the basin scale. This  
 419 approach was used in this application to simulate annual fluctuations in groundwater water  
 420 tables, in Eq. (4), with a period of 1 year, minimums around the middle of the growing season  
 421 (mid-July), and maximums in the cold season (early February). This translates into the lowering  
 422 of the matric potential during the growing season, causing soil water seepage, and an elevated  
 423 matric potential during the non-growing season, causing an increase in the soil moisture  
 424 consistent with field observations. So Thus, thea sine function representing the annual  
 425 fluctuations in the groundwater water table soil ( $G_{y,i}$ ) is defined as below:

426

$$427 \quad G_{y,i} = \left[ A \times \sin \left( \frac{(T_s - D_d \times 24) \times 360}{24 \times 365.25} \right) - B \right] \times f_{y,i} \quad (4)$$

428

429 where  $T_s$  is the time step number,  $D_d$  is a time delay in days,  $A$  is the amplitude of the soil water  
 430 level table (SWFTW/SSS) fluctuation, and  $B$  is an intercept factor.  $f_{y,i}$  is a seasonal factor. The  
 431 sine function coefficient ( $D_d$ ,  $A$ , and  $B$ ) and seasonal factor were adjusted for the whole period  
 432 and for each year through model verification and shown in Table 1. Appendix C provides more  
 433 details on the implementation of Eq. (4).

434

## 435 2.5 Model application and multi-variable, multi-metric validation

436 The study site is a relatively small field, and 2 HRUs ~~revealed~~ were sufficient to capture its  
437 hydrological dynamic in CRHM. The HRUs represent (1) the area immediately upstream of the  
438 outlet where surface ponding occurs (depression storage); and (2) the remaining field (Fig. 3).  
439 The maximum ponding capacity of HRU 1 was estimated using the spatially distributed  
440 hydrodynamic model FLUXOS-OVERFLOW (Costa et al., [2016](#), 2020b). The CRHM model  
441 and new TDM module were set up using the information described in Table 1. Soil textures at  
442 the LON site measured in a 25m grid across three soil depths (0-25 cm, 25-50 cm, and 50-100  
443 cm) averaged 29% sand, 48% silt, and 23% clay (Ontario Ministry of Agriculture, Food and  
444 Rural Affairs Soil Team, unpublished data). This soil grain size distribution corresponds with a  
445 soil-saturated hydraulic conductivity of  $\sim 0.56 \text{ cm h}^{-1}$  ( $\sim 10^{-2.5}$ ) (Garcia-Gutierrez et al., 2018),  
446 which was implemented in CRHM ( $0.5 \text{ cm h}^{-1}$ ), corresponding to a field capacity of 0.03 and  $h_{fc}$   
447 of  $\sim 0.8 \text{ m}$  (Twarskawi et al., 2009, based on a drainage flux of  $0.1 \text{ cm d}^{-1}$ ).

448

449 A robust multi-variable, multi-metric model evaluation strategy was deployed to verify the  
450 capacity of the model to predict tile flow and its impact on the local hydrology. The state  
451 variables examined were tile flow, surface flow, and matric potential. The multi-metric approach  
452 contemplated ~~four~~ five different methods, namely the Nash-Sutcliffe efficiency (*NSE*), Root-  
453 Mean-Square Error (RMSE), Model Bias (Bias), Percentage Bias (PBias), and RMSE-  
454 observation standard deviation ratio (RSR). See Appendix [A-C](#) for more details about the  
455 methodology used. It is generally assumed that  $NSE > 0.50$ ,  $RSR \leq 0.70$ , and *PBias* in the range  
456 of  $\pm 25\%$  are satisfactory for hydrological applications (Moriiasi et al., 2007). Hourly values were

457 used in these calculations, which departs from the daily and monthly analyses typically reported  
 458 for these types of models. Although this is a challenging proposition, it is an important one as it  
 459 constitutes a necessary step forward toward more detailed, accurate, and advanced models for  
 460 these regions. For example, Costa et al., (2021) noted that the successful extension of  
 461 hydrological models to water quality studies relies on their ability to operate at small time scales  
 462 in order to capture intense, short-duration storms that may have a disproportional impact on the  
 463 runoff transport of some chemical species such as phosphorus – in essence, to capture hot spots  
 464 and hot moments for flux generation.

465

466

467 Table 1. Key model parameters in CRHM for representation of the LON site.

468

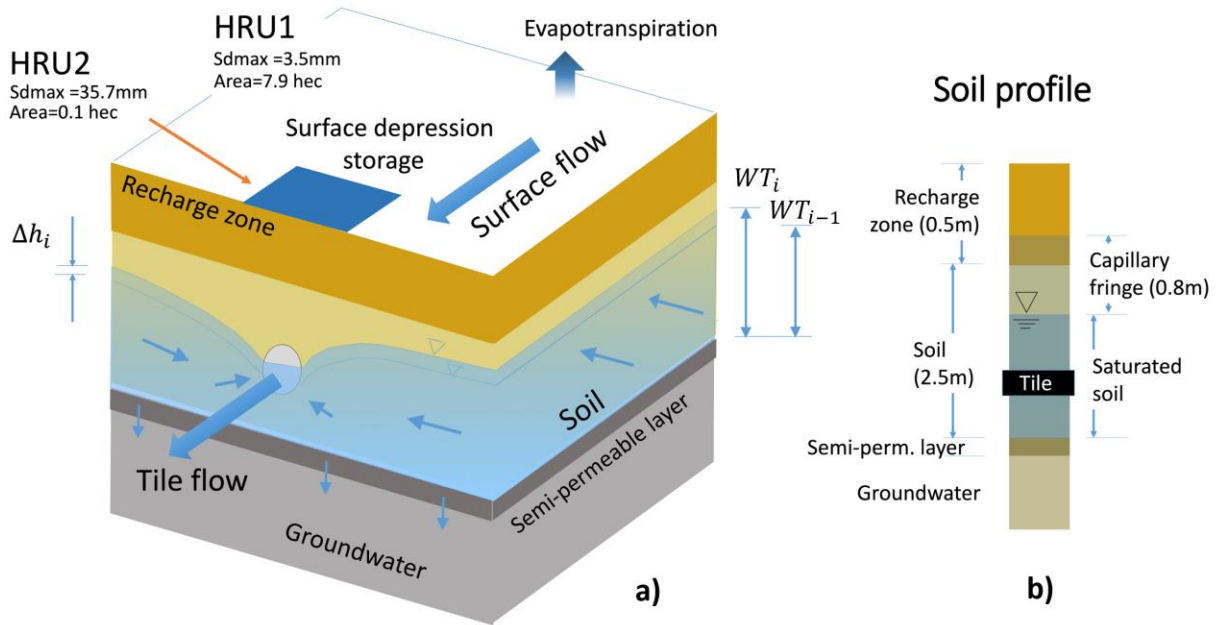
Model Parameter	Value	Unit	Source	Adjusted/Calibrated	Comment
Soil depth	2	m		No	Assumed
Semipermeable layer depth	3	m		No	Assumed
Tile depth	0.9	m		No	Farmer/Blueprints of the field
Corn root depth	0.5	m		No	Online sources
Soil recharge zone- thickness	0.5	m		No	Based on the root depth
Tile spacing	14	m		No	Farmer/Blueprints of the field
Soil porosity (soil drainable water)	0.045			Yes	Adjusted
$\varphi_s$					
K in below layer	5	mm h <sup>-1</sup>		Yes	Adjusted
K in above layer	5	mm h <sup>-1</sup>		Yes	Adjusted
Capillary fringe thickness	0.8	m		Yes	Adjusted

Capillary fringe drainable water $\varphi_c$	0.03		Yes	Adjusted
Surface depression in small area close to farm surface flow outlet (HRU2)	35	mm	Yes	Calculated
Surface depression in rest of the area (HRU1)	<u>0</u>	mm	No	Calculated
Surface area of HRU1	<u>79000</u>	m <sup>2</sup>	No	Field observations and DEM
Surface area of HRU2	<u>1000</u>	m <sup>2</sup>	No	Field observation and DEM
Soil module name in CRHM	WQ_soil		No	
Infiltration module name in CRHM	GreenAmpt		No	
Soil type in GreenAmpt module	5		Yes	Adjusted
Saturated K in GreenAmpt module	6	mm h <sup>-1</sup>	Yes	Adjusted
Soil wilting point	0.025		Yes	Adjusted
A, in sine function	0.025	mm h <sup>-1</sup>	Yes	Adjusted
B, in sine function	-0.005	mm h <sup>-1</sup>	Yes	Adjusted
D <sub>d</sub> , in sine function	15	d	Yes	Adjusted
f <sub>2012,2</sub> (Seasonal factor, sine function)	2.0		Yes	Adjusted
f <sub>2015,2</sub> (Seasonal factor, sine function)	1.8		Yes	Adjusted
f <sub>2016,2</sub> (Seasonal factor, sine function)	2		Yes	Adjusted
f <sub>2017,2</sub> (Seasonal factor, sine function)	1.4		Yes	Adjusted
f <sub>y,i</sub>	1		No	By default for y = 2012 to 2017 and i = 1,2

469

470

471



472

473 Figure 3. a) Schematic conceptual view of the CRHM model configuration, including soil layers, [soil water level table](#)  
 474 [\(SWTWT/SSS\)](#), groundwater, and tile flow.; and b) soil profile, including the capillary fringe and its location relative to the soil  
 475 and tile.

476

### 477 3. Results

478

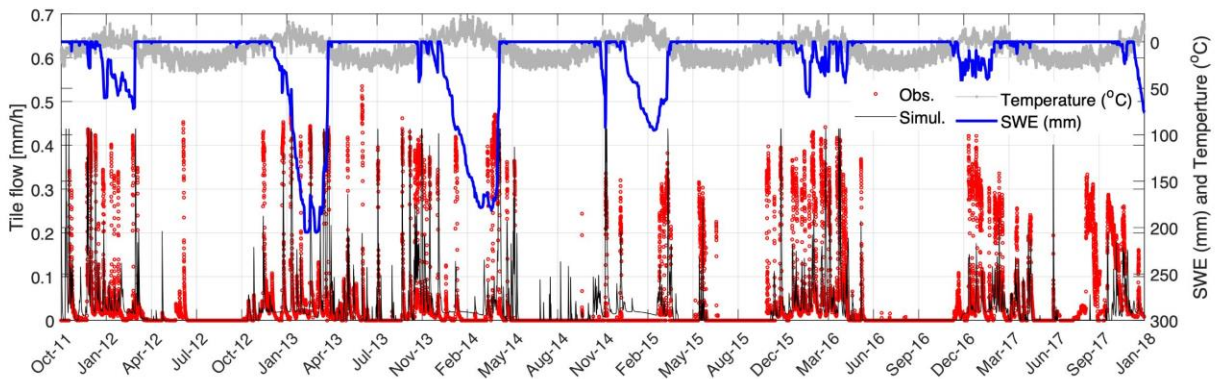
#### 479 3.1 Tile flow

480 The model was able to capture most tile flow events, both in terms of the timing and magnitude  
 481 of peak flows and the most important seasonal patterns (Fig. 4). For example, the almost  
 482 complete absence of tile flow during the growing season (May to September) was captured. The  
 483 simulated flow peaks generally [have had](#) a good agreement with observations, as well as the low  
 484 flow or base flows during cold periods (December-March). The ascending and descending limbs  
 485 of the response signal [are were](#) also adequately predicted.

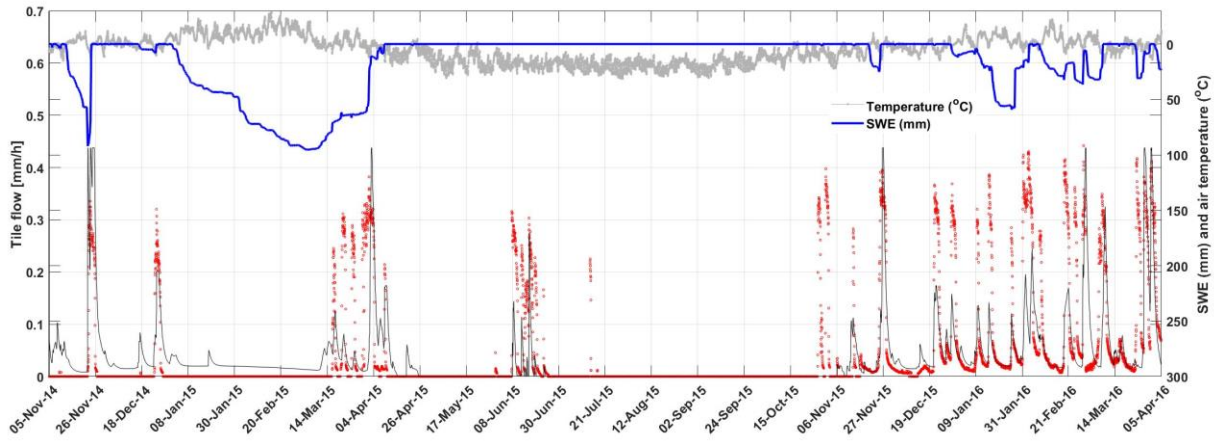
486



487 Results show that tile flows generally occur during snowmelt events, as indicated by the  
488 synchrony between snow water equivalent (SWE) depletion and tile flow. The maximum  
489 snowpacks (or snow water equivalent, SWE) were markedly smaller during the winters of 2016  
490 and 2017 when compared with those of 2013 to 2015. However, this did not necessarily translate  
491 into lower tile flows as precipitation also occurred as rain during these seasons. Although the  
492 magnitude of tile peaks was not always assessed accurately, the model was able to capture the  
493 annual trends of both an absence of tile flow during the summer months (growing season) and  
494 the ascending and descending limbs of the tile hydrograph during events (Figure 4). clearly  
495 shows that the annual general trend in tile flows and the gaps in tile flows during growing  
496 seasons are simulated efficiently. Also, figure 4b shows that how ever all tile flow peaks were  
497 not assessed accurately but the asending and descensinf trend of the tile flow peaks were  
498 simulated accurately.



499  
500 a)



501

502 b)

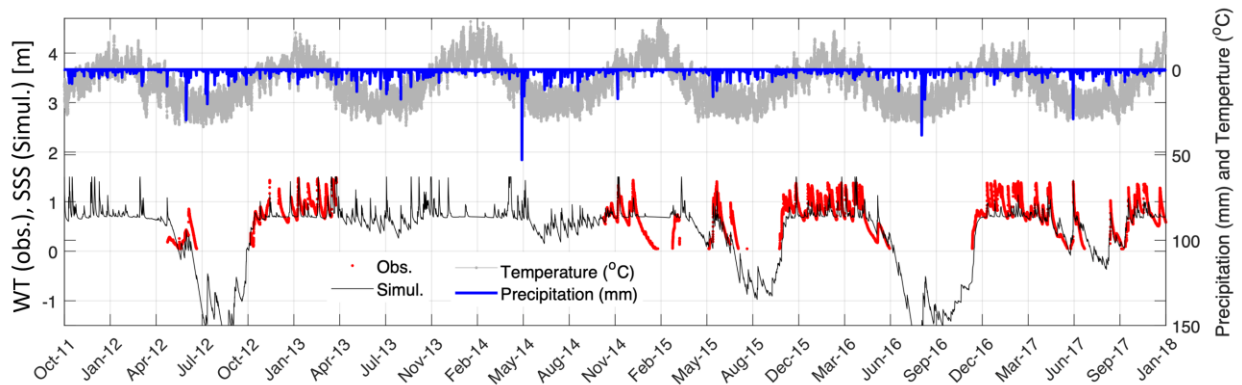
503 Figure 4. Comparison between observed and simulated tile flows, simulated SWE (snow water equivalent), and observed air  
 504 temperature in the LON site.

505

506 3.2 Soil wWater levelstables or soil saturated storage

507 Simulated soil saturated storage and the observed soil-waterwater levels-table position-(m) are  
 508 compared in Fig. 5, alongside air temperature and precipitation observations. Despite the  
 509 observation gaps, the model agrees well with observations. Above tile drains, water table  
 510 fluctuations are controlled by infiltration/recharge, tile flow, groundwater flow, and matric  
 511 potential that affectsaffect the drainable water from the capillary fringe. This causes flashier  
 512 storage responses above the tile that are captured well by the model. In contrast, tiles do not  
 513 withdraw water from the soil layer below the tile pipe and thus do not control water table  
 514 fluctuations when levels are below the drain pipe, and tile drains simply do not flow during such  
 515 periods. This causes flashier soil moisture responses above the tile that are captured well by the  
 516 model. During the growing season, both the observed and simulated soil-waterwater levels  
 517 tables (or saturated storages) drops abruptly because of the seasonal lowering of the regional  
 518 groundwater water table. In the growing seasons of 2012, 2015 and 2016, which were dry years,

519 large [drops/declines](#) in the [soil-waterwater level-table and saturated storage](#) were observed,  
 520 whereas in [other-wetter more-wet](#) years such as 2013 and 2014, seasonal water level declines  
 521 were smaller. The seasonal declines in water level during the growing season led to a cessation  
 522 in tile flow in most years (Fig. 4, 5), even following rainfall events. For example, there was a  
 523 large precipitation event (~35 mm) in the growing season of 2016 that did not produce tile flow  
 524 (apparent in both model and observations).



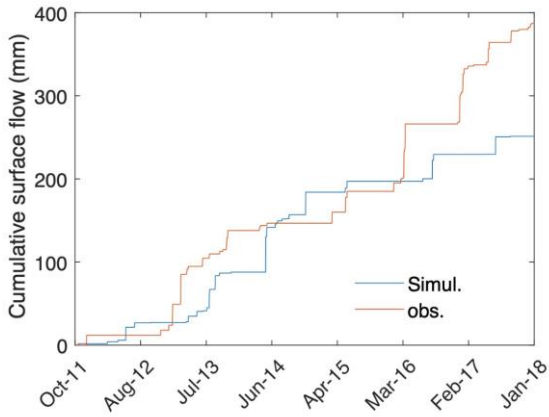
525  
 526 Figure 5. Time series of the simulated [saturated storage](#) and observed [soil-waterwater level-table \(groundwater table\) in soil](#) along  
 527 with the observed temperature and precipitation. The horizontal line shows the depth of the tile pipe.

528  
 529 

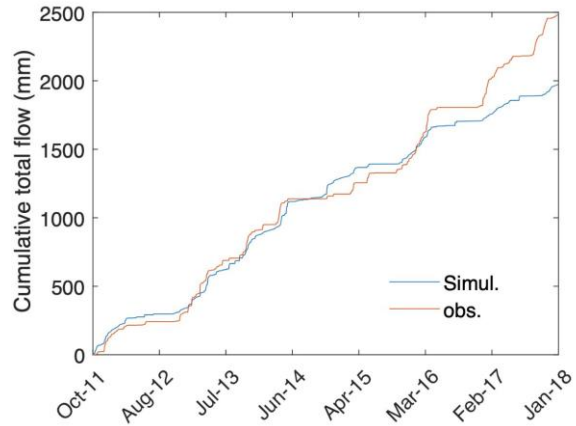
### 3.3 Surface flow and total flow

530 The model was not [always](#) able to capture the observed surface flow as satisfactorily as it  
 531 captured tile drainage (Fig. 6a). Some of the possible reasons are uncertainties in the  
 532 measurements of surface flow due to ponding in surface depressions on the field, which impeded  
 533 the drainage of some of the surface runoff [prior to when it exited the field through the culvert](#)  
 534 (see Fig. 1), [or due to uncertainty in field estimates of SWE](#). However, the model performance  
 535 improves considerably when both runoff and tile flow are combined (referred to as total flow,  
 536 Fig. 6b). Indeed, most of the flow from the field was through tile drains (80% in 5-year average)  
 537 rather than surface runoff (20% in 5-year average, Plach et al., 2019). The underestimation of

538 both cumulative total and surface flows during 2017 and 2018 is possibly due to the removal of  
539 the blockage in the tile pipes in early 2017, thatwhich may have affected both surface and tile  
540 flows.

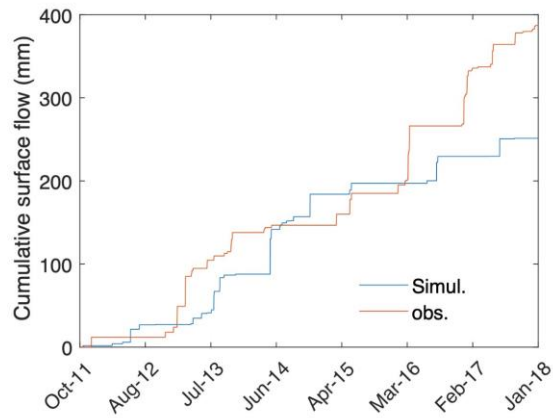


(a)



(b)

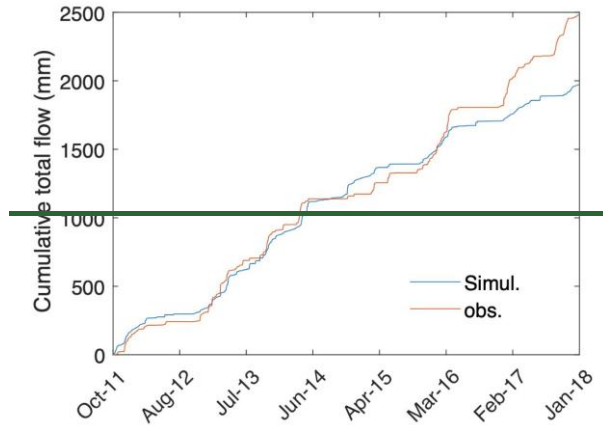
541



542

543

a)



b)

Figure 6. Observed and simulated cumulative surface flow (a) and total flow (b) with their performance coefficients.

### 3.4 Overall model performance

The model performance was calculated based on hourly data for various model outputs (Table 2). The results confirm that the model is robust in the sense that it can capture the main patterns of tile flow, surface flow, and matric potential levels. The PBias values are below 25% for most of the fluxes and cumulative fluxes. The RSR values are also generally below 10.820. The NSE values are positive and above 0.3 for most fluxes, except for surface flow, where the model exhibited some difficulties.

Table 2. Performance coefficients for surface flow, tile flow and soil water water level table (SWTWT/SSS), as well as total (tile + surface) flow and the cumulative surface, tile and tile+surface flows, for the simulation period of October 2011 to January 2018. The coefficients were calculated for both hourly and daily flow rates.

Performance coefficients	Surface flow (mm h <sup>-1</sup> )	Tile flow (mm h <sup>-1</sup> )	SWL SWTWT (-SSS) (m)	Total flow (mm h <sup>-1</sup> )
NSE*	-2.29	0.31	0.49	-1.38

RMSE <sup>△</sup>	0.27	0.08	0.26	0.30
Bias <sup>#</sup>	0.54	0.24	0.14	0.28
PBias <sup>§</sup>	21.77	17.91	10.46	18.63
RSR <sup>&amp;</sup>	1.82	0.83	0.71	1.54
<u>NSE</u>	<u>-0.73</u>	<u>0.29</u>	<u>0.50</u>	<u>0.01</u>
<u>RMSE</u>	<u>2.04</u>	<u>1.72</u>	<u>0.24</u>	<u>2.92</u>
<u>Bias</u>	<u>0.35</u>	<u>0.20</u>	<u>0.09</u>	<u>0.22</u>
<u>PBias</u>	<u>35.11</u>	<u>19.63</u>	<u>9.33</u>	<u>21.73</u>
<u>RSR</u>	<u>1.31</u>	<u>0.84</u>	<u>0.70</u>	<u>0.99</u>

Coefficients calculated  
for daily flow rates  
(mm d<sup>-1</sup>)

<sup>△</sup>Nash-Sutcliffe efficiency, <sup>△</sup>Root-Mean-Square Error, <sup>#</sup>Model Bias, <sup>§</sup>Percentage Bias, <sup>&</sup>RMSE-observation standard deviation ratio

559

560

### 561 3.5 Presence of capillary fringe: effects and hypotheses

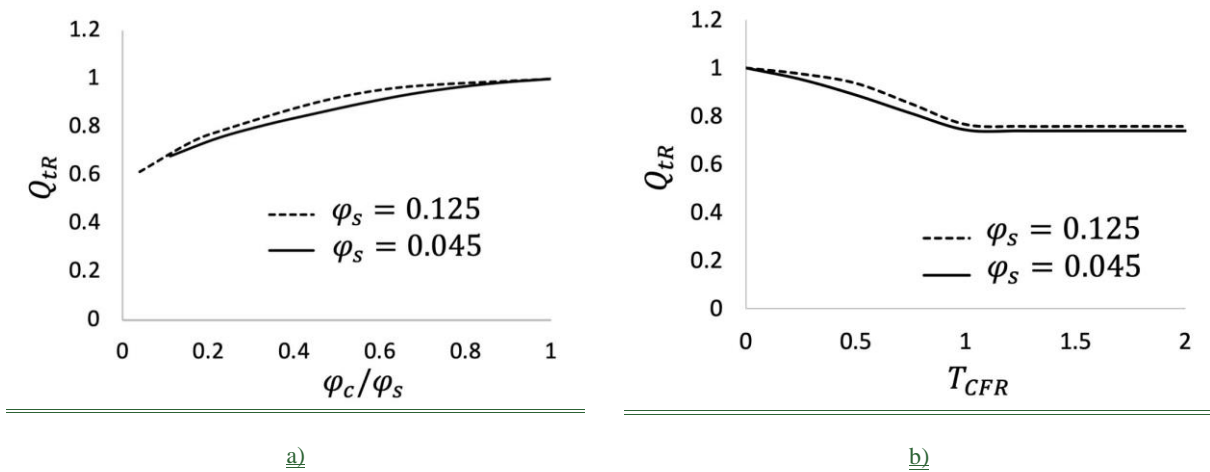
562 Results show that the thickness and vertical positioning of the capillary fringe have a strong  
563 impact on the amount of drainable soil water that can flow into tiles. To investigate this effect  
564 further, ~~we examined~~ the response of ~~the~~ tile flow and soil moisture to changes in the capillary  
565 fringe was investigated. It should be noted that although this thickness may slightly change  
566 depending on the soil type and water retention curves (Skaggs et al., 1978), the model assumed a  
567 constant value given the catchment-scale nature of the simulations and myriad of processes  
568 contemplated. However, despite the simplification, the vertical positioning of the capillary fringe  
569 was still computed and enabled a dynamic (time-dependent) calculation of the drainable soil  
570 water that is available for tile drainage over time.

571

#### 572 Effect of capillary fringe on tile flow

573 Figure 7a relates the simulated normalized total cumulative tile flow ( $Q_{tR}$ , total tile flow divided  
574 by the total tile flow when there is no influence of capillary fringe) to capillary fringe drainable  
575 water ( $\varphi_{CR} = \varphi_c / \varphi_s$ ) for two different  $\varphi_s$  values (0.045 and 0.125). The values were

576 normalized for comparison purposes. As expected, the model indicates that tile flow increases  
 577 with drainable water, but the relationship is non-linear, likely because as tile carrying capacity is  
 578 exceeded more frequently, there is more opportunity for groundwater seepage and  
 579 evapotranspiration. The direct effect of  $\varphi_s$  (comparing the solid and dashed lines) on tile flow is  
 580 small because the amount of water that can effectively drain to the tile is controlled by the  
 581 capillary fringe and the associated drainable soil water. Figure 7b looks at the impact of the  
 582 capillary fringe thickness on tile flow. Here, the values are also normalized. Results show that  
 583  $Q_{tR}$  decreases with increasing normalized thickness of the capillary fringe,  $T_{CFR}$  ( $\frac{T_{CF}}{D_t}$ , capillary  
 584 fringe thickness divided by tile depth), but only while the  $T_{CFR}$  is less than 1 that is when the  
 585 capillary fringe position is above the tile but has not reached the soil surface. Beyond this point,  
 586 increments in the capillary fringe thickness have no impact on tile flow because *Condition 1* has  
 587 been reached (see Fig. 2), which essentially means that the capillary fringe has reached the soil  
 588 surface.



589

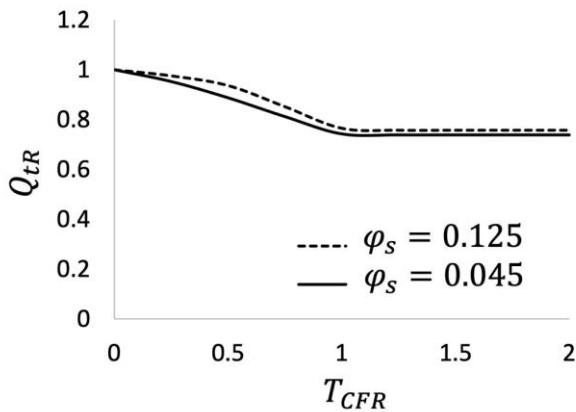
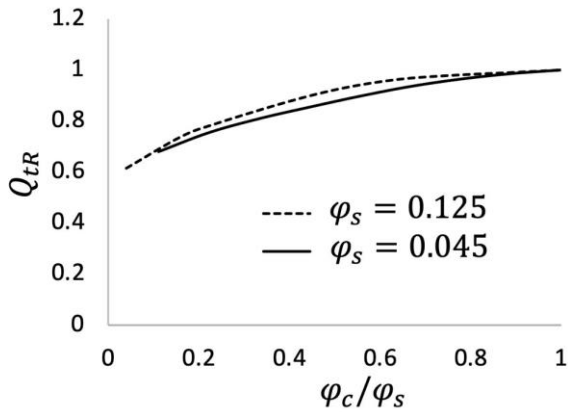


Figure 7. Comparison between normalized tile flow ( $Q_{tR}$ ) and (a) normalized drainable soil water ( $\varphi_c/\varphi_s$ ) and capillary fringe thickness ( $T_{CFR}$ ) for different maximum soil saturation values ( $\varphi_s$ ), [by drawing the model prediction lines](#).

### Effect of capillary fringe on soil moisture

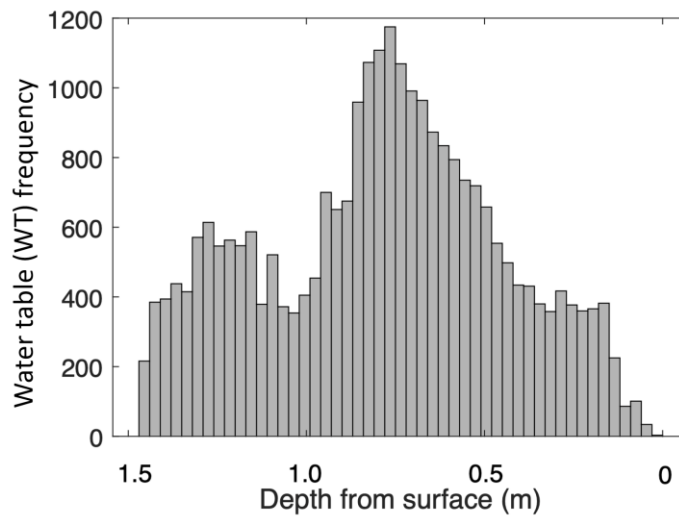
Observations and model results of [SWL-SWFWT](#) (or [SSS](#) as an indicator of soil moisture) reveal a bimodal frequency distribution (Fig. 8 and 9, respectively) with peaks at 0.85 m and 1.25 m depth, with the former corresponding to the depth of the tile pipe and the second peak reflecting capillary fringe thickness. In the simulated [SWL-soil saturated storage \(SSS/SWFWT\)](#) frequency distributions (Fig. 9), the first peak highlights again the efficiency of the tile in removing soil moisture. In contrast, the second peak indicates a strong model response to differences in the



604 capillary fringe thickness. It shows that when there is an-almost-near-constant discharge from the  
605 bottom of the soil layer, the matric potential varies the greatest while it remains between the tile  
606 depth and the soil surface. While the matric potential fluctuates faster and is more unstable  
607 within this range, it also remains there for shorter periods. This bimodal response tends to push  
608 the matric potential below the tile.

609

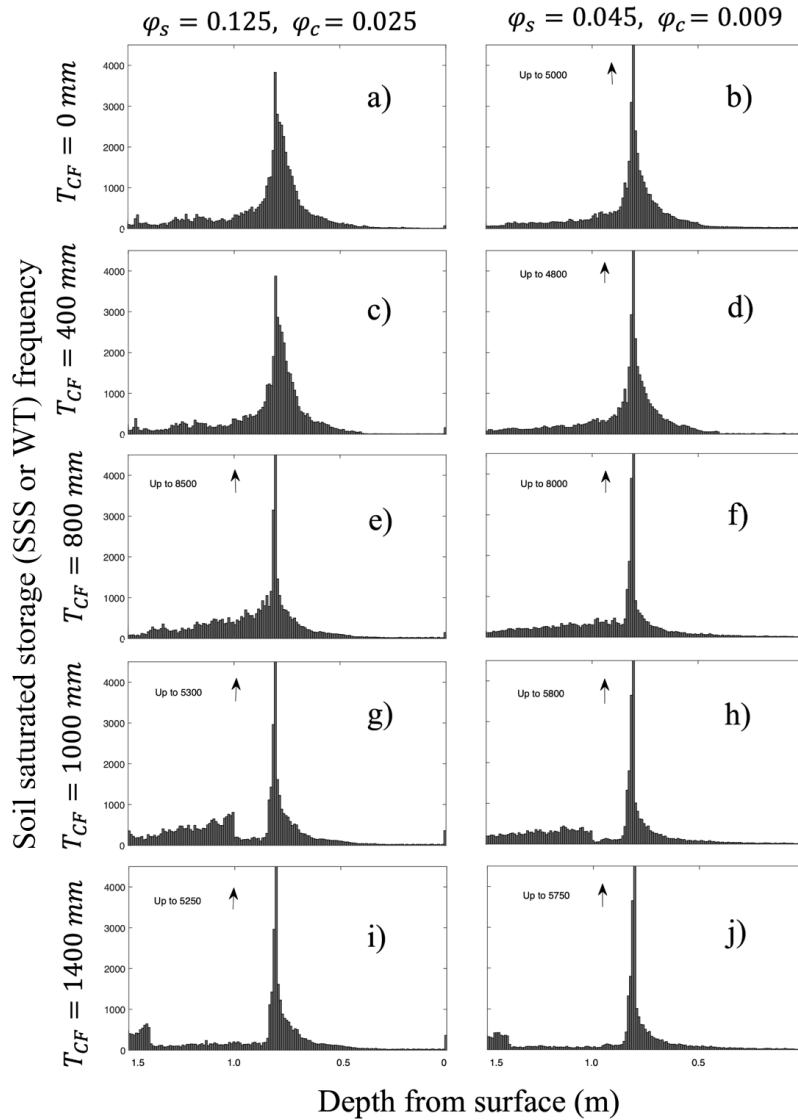
610 The bimodal behavior of the observed soil-waterwater levels-tables and simulated saturated  
611 storage demonstrated here provides the opportunity to quantify the thickness of the capillary  
612 fringe using continuously monitored soil-waterwater levelstable positions. The capillary fringe  
613 thickness determined using this method can then be used as an input to the TDM module.



614

615 Figure 8\_ Histogram of the observed soil-waterwater level-table distribution for the period pf 2011 to 2018 in LON  
616 (Londesborough).

617



618

619

620

621

622

623

#### 624 4. Discussion

625

626

Figure 9. Histograms of the simulated soil saturated storages (soil water levels-SSS or SWFWT) for the capillary fringe thicknesses of 0 (a,b), 400 (c,d), 800 (e,f), 1000 (g,h) and 1400 (i, j) mm and for the  $\phi_s$  and  $\phi_c$  of 0.125 and 0.025 (left column) as well as 0.045 and 0.009 (right column).

The new TDM module developed for CRHM was able to capture tile drainage flow and its effect on the hydrological patterns of a farm field in southern Ontario. This module ~~can~~ helps extend

627 the existing capacity of representing the effect of tile drainage in the hydrology of agricultural  
628 cold regions, from the use of the CRHM platform from agricultural basins in the colder Canadian  
629 Prairies to the more temperate Great Lakes region. Tile drainage is prevalent across much of the  
630 cultivated lands in the Great Lakes basin and adjacent regions from southern Canada to the upper  
631 US Midwest. It is expanding in the eastern Canadian Prairies as well. The new TDM module  
632 will also permit simulating the impacts of a changing climate on runoff processes in these  
633 landscapes. In addition to this potential, the development of the TDM has also provided insights  
634 into hydrological processes in tile-drained landscapes. These are discussed in more detail below.

635

#### 636 4.1 *Insights into key control mechanisms of tile flow for catchment-scale simulations*

637 The model suggests that tile flow may not be accurately ~~simulated~~predicted exclusively based  
638 on the matric potential and soil saturated hydraulic conductivity as suggested by the steady-state  
639 flow assumptions of the Hooghoudt's equation (Hooghoudt, 1940). Our results indicate two  
640 additional controls: (1) the amount of drainable soil water in the soil, which has also been  
641 identified in some field studies (*e.g.*, Skaggs et al., 1978; Moriasi et al., 2013) and (2)  
642 fluctuations in the groundwater table (GWRD) are equally important to account for in  
643 catchment-scale simulations. However, the relationship between drainable water and tile flow  
644 rates is non-linear, as demonstrated in Fig. 7a. This is because the ~~opportunity~~residence time for  
645 groundwater seepage and evapotranspiration increases when the hydraulic tile carrying capacity  
646 is exceeded. Comparatively, the effect of soil drainable water,  $\phi_s$  (see also Fig. 7a) on tile flow is  
647 small because the capillary fringe and associated drainable soil water control the amount of water  
648 that can effectively flow to the tile.

649

650 The verification of the model also indicated that the slopes of the rising and falling limbs of tile  
651 flow hydrographs and [SWL-SWTWT](#) were very sensitive to (1) the ratio between K and  
652 drainable soil water; and (2) the net outflow in the soil through tile flow and groundwater level  
653 fluctuations (GWRD). This is supported by previous studies showing rapid responses of tile  
654 flow to precipitation events (Gentry et al., 2007; Smith et al., 2015) and others that have related  
655 rapid responses in tile discharge to antecedent moisture conditions (Macrae et al., 2007; Vidon  
656 and Cuadra, 2010; Lam et al., 2016a; Macrae et al., 2019), which can be affected by the  
657 development of a capillary fringe and its holding capacity.

658

659 Results show that large fluctuations in [SWL-SWTWT \(or SSS\)](#) and tile flow during the cold  
660 season, when the [soil-waterwater level-table](#) tends to be above the tile, are primarily triggered by  
661 the development of ~~the a~~ capillary fringe that reduces the amount of drainable soil water. Model  
662 sensitivity tests showed that a small amount of drainable soil water produces steeper rising and  
663 falling responses (and with larger fluctuation amplitudes) in both the [soil-waterwater level-table](#)  
664 [\(saturated storage\)](#) and the tile flow. Indeed, this pattern can be observed by exploring  
665 differences in tile drain responses in clay loam soils with larger field capacities (and  
666 correspondingly smaller drainable water) and smaller hydraulic conductivity which are more  
667 likely to experience pronounced oscillations (*e.g.*, steeper rising and falling response curves)  
668 compared to tile drain responses of sandy soil, which is characterized by reduced capillary  
669 forces, lower field capacities (but correspondingly larger drainable water) and higher hydraulic  
670 conductivity. Notably, both model and observations of [SWL-SWTWT/SSS](#) (as a proxy for soil  
671 moisture) reveal a bimodal (*i.e.*, two peaks) frequency distribution when examined in relation to  
672 the tile depth and capillary fringe thickness (Fig. 8 and 9, respectively). The two peaks (*i.e.* most

673 frequently observed ~~SWL~~ SWTWT or SSS conditions) correspond with the (1) depth of the tile  
674 pipe (0.75 m), which demonstrates the efficacy of the tile at rapidly removing excess soil water,  
675 and the (2) the capillary fringe thickness (for the depths of 1.0 and 1.4 m, Figs. g, h, i and j)  
676 beyond which the amount of drainable water above the water level significantly increases.  
677

678 These findings align well with studies such as Lam et al. (2016a) that recorded soil moisture near  
679 saturation after tile flow had ceased, suggesting the development of a capillary fringe. Combined  
680 experimental and modeling works, such as in Moriasi et al. (2013) and Logsdon et al. (2010),  
681 also discuss the impact of drainable soil water (“drainable porosity” or “specific water yield”) on  
682 tile flow and note that the drainable water is, in turn, dependent on the soil type, soil-water  
683 dynamic and ~~soil-water~~ water level table depth. However, these studies did not explore the  
684 dynamic nature of the capillary fringe and its thickness relative to the soil column above in  
685 determining the transient amount of drainage soil water that will impact the ~~SWL~~ SWTWT  
686 distribution and tile flow differently over time (*Conditions 1 to 3*, see Fig. 2). Herein, while ~~we~~  
687 ~~assumed~~ a capillary fringe with a fixed thickness that is generally related to the soil properties  
688 was assumed, its vertical positioning was simulated dynamically, which allowed determining the  
689 drainable soil water based on the evolution of pressure head corresponding to field capacity.

690 Thus, the development of the TDM has provided a step forward in the modeling of tile drainage  
691 ~~at catchment scale~~ and suggests that in loam soils such as those at the study site, the effects of a  
692 capillary fringe on tile flow should be included. Soil moisture (soil unsaturated storage)  
693 measurements from the study site by Van Esbroeck et al., (2017) between November 2011 and  
694 May 2014 from depths of 10, 30, and 50 cm (using EC-5 Soil Moisture Smart Sensor) showed  
695 that almost 90% of the gravitational soil moisture drains out with 0.5 to 2.5 h.

696

697 4.2 Importance of capturing seasonal patterns in groundwater to improve tile flow

698 predictions

699 The GWRD changed dramatically between seasons affecting soil moisture (both saturated and

700 unsaturated storage of the soil) and tile flow patterns. Both observations and model results show

701 that low precipitation and higher evapotranspiration rates tend to produce little tile flow during

702 the growing season. These seasonal patterns in precipitation and evapotranspiration are

703 accompanied by a reduction in soil moisture (both unsaturated storage and saturated storage soil

704 water level) that leads to a substantial storage capacity in fields. Even following moderate and

705 high-intensity storms during the growing season, rapid soil moisture (~~both saturated and~~

706 ~~unsaturated storage of the soil~~) increases are observed (both saturated and unsaturated soil

707 storage); however, tile flow rarely develops, suggesting that the soil is able to hold the water

708 (Lam et al., 2016a; Van Esbroeck et al., 2016). In contrast, tile flow is often observed during the

709 cold season, even during smaller rainfall-runoff and snowmelt events because of reduced soil

710 storage but also a seasonal increase in GWRD (Lam et al., 2016a; Macrae et al., 2007, 2019; Van

711 Esbroeck et al., 2016). This concurs with several studies throughout the Great Lakes and St.

712 Lawrence region that have reported stronger tile responses during the non-growing season, with

713 the summer months often showing little to no tile flow (Lam et al., 2016a, 2016b; Jamieson et

714 al., 2003; Macrae et al., 2007; Hirt et al., 2011; King et al., 2016; Van Esbroeck et al., 2016;

715 Plach et al., 2019).

716

717 These results (the controlling effect of soil drainable water and groundwater level fluctuations on

718 tile flow) suggest that while soil moisture (both SSS and unsaturated storage) is largely

719 controlled by tile flow rather than GWRD in the cold season, this reverses in the growing season  
720 (~~i.e.i.e.~~, soil moisture controls tile flow), ~~and,with~~ soil moisture (both SSS and unsaturated  
721 storage) ~~is-being~~ also impacted by evapotranspiration. The controlling effect of groundwater  
722 fluctuations in the growing season has also been studied by Hansen et al., (2019). The model  
723 indicated that the rapid drops ~~the~~ observed in ~~SWL~~ SWTWT during the growing season could  
724 not be explained by evapotranspiration alone as well as the crop root depths, thus pointing ~~at~~  
725 the role of GWRD. Johnsen et al. (1995) and Akis (2016) also showed that the effect of  
726 groundwater accretion was more effective on tile flows than ~~the~~ surface runoff. Also, Vaughan et  
727 al. (1999) found that ~~in their study site the~~ tile drain flows in their study site in ~~the~~ San Joaquin  
728 Valley of California ~~iswere more~~ better explained and related to nonlocal groundwater  
729 appearance ~~rather than to~~ local variations in irrigation amount, evapotranspiration, variation in  
730 water storage or tile drain blockage.

731

## 732 5. Conclusion

733 A new tile drain module within the modular Cold Regions Hydrological Modelling platform has  
734 been created and tested ~~for catchment scales~~ at the single field scale ~~site simulations within the~~  
735 ~~modular Cold Regions Hydrological Modelling platform~~ to support the management of  
736 agricultural basins with seasonal snow covers ~~support management in agricultural basins that~~  
737 ~~have seasonal snow covers~~. The model was tested and validated for a small working farm in  
738 southern Ontario, Canada, and presents a step forward in the dynamic simulation of tile flow and  
739 its effects on the hydrological cycle in cold climates. Observations and model results showed that  
740 the dynamic prediction of tile flow and soil moisture (~~SSS/SWTWT~~) at catchment scales needs  
741 to account for (1) the amount of drainable soil water that can be affected by the development of a

742 capillary fringe and (2) fluctuations in the groundwater water table, in addition to the typical (3)  
743 matric potential above the tile pipe and (4) the soil saturated hydraulic conductivity considered  
744 by the steady-state flow Hooghoudt's equation.

745

746 The groundwater table and matric potential changed dramatically between seasons, affecting  
747 patterns of soil moisture ~~( $SWTWT/SSS$ )~~ and tile flow. Observations and model results showed  
748 that low precipitation and higher evapotranspiration rates caused minimal tile flows during the  
749 crop-growing season. Conversely, tile flow was often observed during the cold season, even  
750 during small rainfall-runoff and snowmelt events due to a seasonal increase in the groundwater  
751 table and soil ~~saturated storage ( $SWTWT/SSS$  water level)~~.

752

753 Model sensitivity tests showed that the capillary fringe strongly affected the amount of drainable  
754 soil water flowing into the tile. Tile flow increased with drainable water, but the relationship is  
755 highly non-linear likely because, as the tile carrying capacity is exceeded more frequently, there  
756 is more opportunity time for groundwater seepage and evapotranspiration. Finally, observations  
757 and model results reveal a bimodal soil ~~moisture-saturated storage ( $SSS/SWTWT$ )~~ response in  
758 the presence of tiles, which is controlled by the relative positioning of the capillary fringe in  
759 relation to the soil surface and ~~the depth of tile pipedrain~~ below the soil surface. Capturing these  
760 dynamics is a critical advance enabling the accurate prediction of the swift hydrological changes  
761 caused by the presence of tiles in ~~catchment-scale~~ models.

762 The TDM was developed as a first approximation from a single field site. Given this limitation, it  
763 is not widely applicable across multiple field sites yet. However, the development of this module  
764 has provided valuable insight into the potential for hourly ~~time-step simulations~~ time steps, as



765 well as the importance of regional groundwater table fluctuations and simplifying the capillary  
766 fringe parameters within models in some landscape types. ~~As the next steps~~Future work will  
767 includes building on the model and adapting it for different soil textures such as those in clay  
768 soils, where ~~representing preferential flow in the model as this phenomenon~~ can have a strong  
769 impact on soil ~~moisture~~saturated storage ~~affecting~~and tile flow ~~we want to focus first on~~  
770 calibration and validation of our results and improve the module by adding the preferential flow  
771 to it. Also, explicit representation of unsaturated flow ~~another aspect that should be consider in~~  
772 our future work would be to count the delays in drainage of soil moisture from the unsaturated  
773 part of the soil will be needed to enable the use of the model regions where groundwater is  
774 disconnected from surface water, as commonly happens in arid and semi-arid regions.  
775 Subsequent steps include the development of water quality modules.

776

### 777 Code/Data ~~availibility~~availability

778 The tile flow and soil water table data are not publicly available and will be provided upon  
779 request to the data owner, Merrin Macrae. TDM code is not completely implemented in the main  
780 version of the Cold Regions Hydrological Model platform ~~yet~~ and is provided only upon request  
781 to the corresponding author.

782

### 783 **Author contribution**

784 MK and DC developed the model code and performed the simulations. MM prepared the data  
785 and supported the field work. MK, ~~and~~DC and MM prepared the manuscript with contributions  
786 of ~~from~~ MM, JP and RP.

787

788 **Competing interests**

789 The contact author has declared that none of the authors has any competing interests.

790

791 **Acknowledgements**

792 Funding for this project was provided by the Canada First Excellence Research Fund's Global  
793 Water Futures programme through its Agricultural Water Futures project. Funding for the  
794 collection of the field data was provided by the Ontario Ministry of Agriculture, Food and Rural  
795 Affairs. The support of the Biogeochemistry Lab at the University of Waterloo for the collection  
796 of field data and of Tom Brown and Xing Fang of the Centre for Hydrology at the University of  
797 Saskatchewan for CRHM development and updates is gratefully acknowledged. The Maitland  
798 Valley Conservation Authority is thanked for providing some precipitation, ~~rainfall~~rainfall, and  
799 temperature data.

800

801 **References**

802 Akis R.: Simulation of Tile Drain Flows in an Alluvial Clayey Soil Using HYDRUS 1D,

803 American-Eurasian J. Agric. & Environ. Sci., 16 (4), 801-813,

804 <https://doi.org/10.5829/idosi.aejaes.2016.16.4.12906>, 2016.

805

806 Arheimer, B., Nilsson, J., and Lindstrom, G.: Experimenting with Coupled Hydro-Ecological  
807 Models to Explore Measure Plans and Water Quality Goals in a Semi-Enclosed Swedish Bay,  
808 Water, 7(7), 3906-3924, <https://doi.org/10.3390/w7073906>, 2015.

809

810 Arnold, J. G., Srinivasan, R., Muttiah, R. S., and Williams, J. R.: Large area hydrologic  
811 modeling and assessment part I: model development, J. Am. Water. Resour. Assoc., 34, 73-89,  
812 <https://doi.org/10.1111/j.1752-1688.1998.tb05961.x>, 1998.  
813

814 Badr, A. W.: Physical properties of some North Carolina Organic Soils and the effect of land  
815 development on these properties, M.S. Thesis, Department of Biological and Agricultural  
816 Engineering, North Carolina State University, Raleigh, NC. 67 p., 1978.  
817

818 Blear, W. (2<sup>nd</sup> Edition): Soil and Environmental Chemistry, Academic Press, eBook ISBN:  
819 9780128041956, 2017.  
820

821 Bouwer, H. and van Schilfhaarde, J.: Simplified method of predicting the fall of water table in  
822 drained land, Trans. ASAE. 6(4), 288-291, 296, 1963.  
823

824 Brockley, R. P.: The effect of nutrient and moisture on soil nutrient availability, nutrient uptake,  
825 tissue nutrient concentration, and growth of Douglas-Fir seedlings, Master Thesis, The  
826 University of British Columbia, 1976.  
827

828 Broughton, R. and Jutras, P.: Farm Drainage. In the Canadian Encyclopedia,  
829 <https://www.thecanadianencyclopedia.ca/en/article/farm-drainage/>, last access: 14 February  
830 2019.  
831

832 Coelho, B. B., Murray, R., Lapen, D., Topp, E., and Bruin, A.: Phosphorus and sediment loading  
833 to surface waters from liquid swine manure application under different drainage and tillage  
834 practices, *Agric. Water Manag.*, 104, 51-61, <https://doi.org/10.1016/j.agwat.2011.10.020>, 2012.

835

836 Cordeiro, M. R. C. and Ranjan, R. S.: Corn yield response to drainage and subirrigation in the  
837 Canadian Prairies, *Trans. ASABE*. 55(5), 1771-1780, <https://doi.org/10.13031/2013.42369>,  
838 2012.

839

840 Cordeiro, M. R. C., Wilson, H. F., Vanrobaeys, J., Pomeroy, J. W., Fang, X., and The Red-  
841 Assiniboine Project Biophysical Modeling Team: Simulating cold-region hydrology in an  
842 intensively drained agricultural watershed in Manitoba, Canada, using the Cold Region  
843 Hydrological Model, *Hydrol. Earth Syst. Sci.*, 21, 3483-3506, [https://doi.org/10.5194/hess-21-  
844 3483-2017](https://doi.org/10.5194/hess-21-3483-2017), 2017.

845

846 Correll, D.: The role of phosphorus in the eutrophication of receiving waters: a review, *J.*  
847 *Environ. Qual.*, 27, 261-266, <https://doi.org/10.2134/jeq1998.00472425002700020004x>, 1998.

848

849 [Costa D., Klenk K., Knoblen W., Ireson A., Spiteri, R., Clark, M.: A multi-chemistry modelling  
850 framework to enable flexible and reproducible water quality simulations in existing hydro-  
851 models: 1. The OpenWQ concept and the water quality modelling lab. ESS Open Archive.  
852 <https://10.22541/essoar.168718167.75677635/v1>, 2023](https://doi.org/10.22541/essoar.168718167.75677635/v1)

853

854 [Diogo Costa, Kyle Klenk, Wouter Johannes Maria Knoben, et al. A multi-chemistry modelling](#)  
855 [framework to enable flexible and reproducible water quality simulations in existing hydro-](#)  
856 [models: 2. The OpenWQ-SUMMA and OpenWQ-CRHM model implementations and testing.](#)  
857 [ESS Open Archive. <https://10.22541/essoar.168652285.59958331/v1>, 2023.](#)

858  
859 [Costa, D., Sutter, D., Shepherd, A., Jarvie, H., Wilson, H., Elliott, J., Liu, J., and Macrae, M.:](#)  
860 [Impact of climate change on catchment nutrient dynamics: insights from around the](#)  
861 [world. \*Environmental Reviews\*. \*\*31\*\*\(1\): 4-25. <https://doi.org/10.1139/er-2021-0109>, 2022](#)

862  
863 Costa, D., Baulch, H., Elliott, J., Pomeroy, J., and Wheeler, H.: Modelling nutrient dynamics in  
864 cold agricultural catchments: A review, *Environ. Model. Softw.*, 124, 104586,  
865 <https://doi.org/10.1016/j.envsoft.2019.104586>, 2020a.

866  
867 Costa, D., Shook, K., Spence, C., Elliott, J., Baulch, H., Wilson, H., and Pomeroy, J.: Predicting  
868 variable contributing areas, hydrological connectivity, and solute transport pathways for a  
869 Canadian Prairie basin, *Water Resour. Res.*, 56, 1-23, <https://doi.org/10.1029/2020WR02798>,  
870 2020b.

871  
872 [Costa, D., Burlando, P., Liong, S.-Y.: Coupling spatially distributed river and groundwater](#)  
873 [transport models to investigate contaminant dynamics at river corridor scales. \*Environmental\*](#)  
874 [Modelling & Software, \*\*86\*\*, 91–110. <https://doi.org/10.1016/j.envsoft.2016.09.009>, 2016](#)

875  
876 Costa, D., Pomeroy, J. W., Brown, T., Baulch, H., Elliott, J., and Macrae, M.: Advances in the  
877 simulation of nutrient dynamics in cold climate agricultural basins: Developing new nitrogen and

878 phosphorus modules for the Cold Regions Hydrological Modelling Platform, J. Hydrol., 603, 1-  
879 17, <https://doi.org/10.1016/j.jhydrol.2021.126901>, 2021.

880  
881 [Clark, M. P., Nijssen, B., Lundquist, J. D., Kavetski, D., Rupp, D. E., Woods, R. A., Freer, J. E.,](#)  
882 [Gutmann, E. D., Wood, A. W., Brekke, L. D., Arnold, J. R., Gochis, D. J., & Rasmussen, R. M.](#)  
883 [\(2015\). A unified approach for process-based hydrologic modeling: 1. Modeling concept. Water](#)  
884 [Resources Research, 51\(4\), 2498–2514. <https://doi.org/https://doi.org/10.1002/2015WR017198>](#)

885  
886 [Clark, M. P., Nijssen, B., Lundquist, J. D., Kavetski, D., Rupp, D. E., Woods, R. A., Freer, J. E.,](#)  
887 [Gutmann, E. D., Wood, A. W., Gochis, D. J., Rasmussen, R. M., Tarboton, D. G., Mahat, V.,](#)  
888 [Flerchinger, G. N., & Marks, D. G. \(2015\). A unified approach for process-based hydrologic](#)  
889 [modeling: 2. Model implementation and case studies. Water Resources Research, 51\(4\), 2515–](#)  
890 [2542. <https://doi.org/https://doi.org/10.1002/2015WR017200>](#)

891  
892 De Ridder, N. A., Takes, C. A. P., van Someren, C. L., Bos, M. G., Messemaeckers van de  
893 Graaff, R. H., Bokkers, A. H. J., Stransky, J., Wiersma-Roche, M. F. L., and Beekman, T.:  
894 Drainage Principles and Applications. International Institute for Lan Reclamation and  
895 Improvement, P.O. Box 45 Wageningen The Netherlands, 1974.

896  
897 Du, B., Arnold, J. G., Saleh, A., and Jaynes, D. B.: Development and application of SWAT to  
898 landscapes with tiles and potholes, Trans. ASAE, 48, 1121-1133,  
899 <https://doi.org/10.13031/2013.18522>, 2005.

900

901 Du, B., Saleh, A., Jaynes, D. B., and Arnold, J. G.: Evaluation of SWAT in simulating nitrate  
902 nitrogen and atrazine fates in a watershed with tiles and potholes, Trans. ASABE, 49, 949-959,  
903 <https://doi.org/10.13031/2013.21746>, 2006.

904  
905 ECCC, Canadian Climate Normals 1981-2010 Station Data,  
906 [https://climate.weather.gc.ca/climate\\_normals/results\\_1981\\_2010\\_e.html?searchType=stnProx&txtRadius=25&selCity=&selPark=&optProxType=custom&txtCentralLatDeg=43&txtCentralLatMin=41&txtCentralLatSec=55&txtCentralLongDeg=81&txtCentralLongMin=28&txtCentralLongSec=47&txtLatDecDeg=&txtLongDecDeg=&stnID=4545&dispBack=0](https://climate.weather.gc.ca/climate_normals/results_1981_2010_e.html?searchType=stnProx&txtRadius=25&selCity=&selPark=&optProxType=custom&txtCentralLatDeg=43&txtCentralLatMin=41&txtCentralLatSec=55&txtCentralLongDeg=81&txtCentralLongMin=28&txtCentralLongSec=47&txtLatDecDeg=&txtLongDecDeg=&stnID=4545&dispBack=0), last access: 5  
909 February 2020.

910  
911  
912 Eckersten, H., Jansson, P. -E., and Johnsson, H. (2<sup>nd</sup> edition): SOILN model-user's manual,  
913 Division of Agricultural Hydrotechnics Communications 94:4, Department of soil Sciences,  
914 Swedish University of Agricultural Sciences, 58pp, Uppsala, 1994.

915  
916 Environment Canada, Canadian Climate Normals 1981-2010 Station Data,  
917 [https://climate.weather.gc.ca/climate\\_data/daily\\_data\\_e.html?hlyRange=%7C&dlyRange=1966-06-01%7C2021-06-14&mlyRange=1966-01-01%7C2006-12-01&StationID=4603&Prov=ON&urlExtension=e.html&searchType=stnName&optLimit=yearRange&StartYear=1840&EndYear=2022&selRowPerPage=25&Line=0&searchMethod=contains&Month=6&Day=4&txtStationName=Wroxeter&timeframe=2&Year=2021](https://climate.weather.gc.ca/climate_data/daily_data_e.html?hlyRange=%7C&dlyRange=1966-06-01%7C2021-06-14&mlyRange=1966-01-01%7C2006-12-01&StationID=4603&Prov=ON&urlExtension=e.html&searchType=stnName&optLimit=yearRange&StartYear=1840&EndYear=2022&selRowPerPage=25&Line=0&searchMethod=contains&Month=6&Day=4&txtStationName=Wroxeter&timeframe=2&Year=2021), last access: 10  
921 May 2020.

923

924 Fang, X., Pomeroy, J. W., Westbrook, C. J., Guo, X., Minke, A. G., and Brown, T.: Prediction of  
925 snowmelt derived streamflow in a wetland dominated prairie basin, *Hydrol. Earth Syst. Sci.*, 14,  
926 991-1006, <https://doi.org/10.5194/hess-14-991-2010>, 2010.

927

928 Fang, X., Pomeroy, J. W., Ellis, C. R., MacDonald, M. K., DeBeer, C. M., and Brown, T.: Multi-  
929 variable evaluation of hydrological model predictions for a headwater basin in the Canadian  
930 Rocky Mountains, *Hydrol. Earth Syst. Sci.*, 17, 1635-1659, [https://doi.org/10.5194/hess-17-](https://doi.org/10.5194/hess-17-1635-2013)  
931 [1635-2013](https://doi.org/10.5194/hess-17-1635-2013), 2013.

932

933 Filippelli, G. M.: The global phosphorus cycle, *Rev. Mineral. and Geochem.*, 48, 391-425,  
934 <https://doi.org/10.2138/rmg.2002.48.10>, 2002.

935

936 Frey, S. K., Hwang, H. T., Park, Y. J., Hussain, S. I., Gottschall, N., Edwards, M., and Lapen, D.  
937 R.: Dual permeability modeling of tile drain management influences on hydrologic and nutrient  
938 transport characteristics in macroporous soil, *J. Hydrol.*, 535, 392-406,  
939 <http://dx.doi.org/10.1016/j.jhydrol.2016.01.073>, 2016.

940

941 Gentry, L. E., David, M. B., Royer, T. V., Mitchell, C. A., and Starks, K.: Phosphorus transport  
942 pathways to streams in tile-drained agricultural watersheds, *J. Environ. Quality.*, 36, 408-415,  
943 <https://doi.org/10.2134/jeq2006.0098>, 2007.

944



945 Garcia-Gutierrez, C., Pachepsky, Y., and Martin, M. A.: Technical note: Saturated hydraulic  
946 conductivity and textural heterogeneity of soils, *Hydrol. Earth Syst. Sci.*, 22, 3923-3932,  
947 <https://doi.org/10.5194/hess-22-3923-2018>, 2018.

948

949 Green, C. H., Tomer, M. D., Di Luzio, M., and Arnold, J. G.: Hydrologic evaluation of the Soil  
950 and Water Assessment Tool for large tile-drained watershed in Iowa, *Trans. ASABE.*, 49, 413-  
951 422, <https://doi.org/10.13031/2013.20415>, 2006.

952

953 [Hansen, A. L., Jakobsen, R., Refsgaard, J. C., Hojberg, A. L., Iversen, B. V., and Kjaergaard, C.:  
954 Groundwater dynamics and effect of tile drainage on water flow across the redox interface in a  
955 Danish Weichsel till area, \*Advances in Water Resources\*, 123, 23-39,  
956 <https://doi.org/10.1016/j.advwatres.2018.10.022>, 2019.](#)

957

958 Hirt, U., Wetzig, A., Amatya, M. D., and Matranga, M.: Impact of seasonality on artificial  
959 drainage discharge under temperate climate conditions, *Int. Rev. Hydrobiol.*, 96, 561-577,  
960 <https://doi.org/10.1002/iroh.201111274>, 2011.

961

962 Hooghoudt, S. B.: Bijdrage tot de kennis van enige natuurkundige grootheden van de grond.  
963 *Verslagen van Landbouwkundige Onderzoekingen*, 46(7), 515-707, the Hague, The Netherlands  
964 (in Dutch), 1940.

965

966 ICID: World Drained Area-2018. International Commission on Irrigation and Drainage.  
967 <http://www.icid.org/world-drained-area.pdf> , last access: 14 February 2019.

968  
969  
970  
971  
972  
973  
974  
975  
976  
977  
978  
979  
980  
981  
982  
983  
984  
985  
986  
987  
988  
989  
990

Jamieson, A., Madramootoo, C. A., and Enright, P.: Phosphorus losses in surface and subsurface runoff from a snowmelt event on an agricultural field in Quebec, *Can. Biosyst. Eng.*, 45, 11-17, 2003.

Jarvie, H. P., Johnson, L. T., Sharpley, A. N., Smith, D. R., Baker, D. B., Bruulsema, T. W., and Confesor, R.: Increased Soluble Phosphorus Loads to Lake Erie: Unintended Consequences of Conservation Practices?, *J. Environ. Qual.*, 46, 123-132, <https://doi.org/10.2134/jeq2016.07.0248>, 2017.

Javani-Jouni, H., Liaghat, A., Hassanoghli, A., and Henk, R.: Managing controlled drainage in irrigated farmers' fields: A case study in the Moghan Plain, Iran, *Agric. Water Manag.*, 208, 393-405, <https://doi.org/10.1016/j.agwat.2018.06.037>, 2018.

[Johnsen, K. E., Liu, H. H., Dane, J. H., Ahuja, L. R., and Workman, S. R.: Simulating Fluctuating Water Tables and Tile Drainage with a Modified Root Zone Water Quality Model and a New Model WAFLOWM, \*Transactions of the ASAE\*, 38 \(1\), 75-83, <https://doi.org/10.10031/2013.27814>, 1995.](https://doi.org/10.10031/2013.27814)

Kiesel, J., Fohrer, N., Schmalz, B., and White, M. J.: Incorporating landscape depressions and tile drainages of a northern German lowland catchment into a semi-distributed model, *Hydrol. Process.*, 24, 1472-1486, <https://doi.org/10.1002/hyp.7607>, 2010.

991 King, K. W., Williams, M. R., Macrae, M. L., Fausey, N. R., Frankenberger, J., Smith, D. R.,  
992 Kleinman, P. A. J., and Brown, L. C.: Phosphorus transport in agricultural subsurface drainage:  
993 A review, *J. Environ. Qual.*, 44(2), 467-485, <https://doi.org/10.2134/jeq2014.04.0163>, 2015.  
994  
995 King, K. W., Williams, M. R., and Fausey, N. R.: Effect of crop type and season on nutrient  
996 leaching to tile drainage under a corn-soybean rotation, *J. Soil and Water Conserv.*, 71, 56-68,  
997 <https://doi.org/10.2489/jswc.71.1.56>, 2016.  
998  
999 Kirkham, D.: Theory of land drainage, in, *Drainage of Agricultural Lands*. Agronomy  
1000 Monograph, No. 7, American Society of Agronomy, Madison, Wisconsin, 1957.  
1001  
1002 Kladivko, E. J., Grochulska, J., Turco, R. F., Van Scoyoc, G. E., and Eigel, J. D.: Pesticide and  
1003 nitrate transport into subsurface tile drains of different spacings, *J. Environ. Qual.*, 28, 997-1004,  
1004 <https://doi.org/10.2134/jeq1999.00472425002800030033x>, 1999.  
1005  
1006 Klaiber, L. B., Kramer, S. R., and Young, E. O.: Impacts of Tile Drainage on Phosphorus Losses  
1007 from Edge-of-field Plots in the Lake Champlain Basin of New York, *Water*, 12, 328,  
1008 <https://doi.org/10.3390/w12020328>, 2020.  
1009  
1010 Kock, S., Bauwe, A., and Lennartz, B.: Application of SWAT Model for a Tile-Drained Lowland  
1011 Catchment in North-Eastern Germany on Subbasin Scale, *Water Resour. Manage.*, 27, 791-805,  
1012 <https://doi.org/10.1007/s11269-012-0215-x>, 2013.  
1013

1014 Kokulan, V.: Environmental and Economic Consequences of Tile Drainage Systems in Canada,  
1015 The Canadian Agri-Food Policy Institute (CAPI), 2019.  
1016  
1017 Kokulan, V., Macrae, M. L., Ali, G. A., and Lobb, D. A.: Hydroclimatic controls on runoff  
1018 activation in a artificially drained, near-level vertisolic clay landscape in a Prairie climate, *Hyrol.*  
1019 *Process.*, 33, 602-615, <https://doi.org/10.1002/hyp.13347>, 2019a.  
1020  
1021 Lam, W. V., Macrae, M. L., English, M. C., O'Halloran, I. P., Plach, J. M., and Wang, Y.:  
1022 Seasonal and event-based drives of runoff and phosphorus export through agricultural tile drains  
1023 under sandy loam soil in a cool temperate region, *Hydrol. Process.*, 30, 2644-2656,  
1024 <https://doi.org/10.1002/hyp.10871>, 2016a.  
1025  
1026 Lam, W. V., Macrae, M. L., English, M. C., O'Halloran, I., and Wang, Y.: Effects of tillage  
1027 practices on phosphorus transport in tile drain effluent in sandy loam agricultural soils in  
1028 Ontario, Canada, *J. Great Lakes Res.*, 42(6), 1260-1270,  
1029 <https://dx.doi.org/10.1016/j.jglr.2015.12.015>, 2016b.  
1030  
1031 Larsbo, M., and Jarvis, N.: MACRO 5.0. A model of water flow and solute transport in  
1032 microporous soil, Technical description. Swedish University of Agricultural Sciences, Division  
1033 of Environmental Physics, Emergo 2003:6 Report, ISSN 1651-7210, ISBN 91-576-6592-3,  
1034 2003.  
1035

1036 Lindstrom, G., Pers, C., Rosberg, J., Stromqvist, J., and Arheimer, B.: Development and testing  
1037 of the HYPE (Hydrological Predictions for the Environment) water quality model for different  
1038 scales, *Hydrol. Res.*, 41(3-4), 295-319, <https://doi.org/10.2166/nh.2010.007>, 2010.

1039

1040 Logsdon, S. D., Schilling, K. E., Hernandez-Ramirez, G., Prueger, J. H., Hatfield, J. L., and  
1041 Sauer, T. J.: Field estimation of specific yield in a central Iowa crop field, *Hydrol. Process.*, 24,  
1042 1369-1377, <https://doi.org/10.1002/hyp.7600>, 2010.

1043

1044 Macrae, M. L., English, M. C., Schiff, S. L., and Stone, M. L.: Intra-annual variability in the  
1045 contribution of tile drains to basin discharge and phosphorus export in a first order agricultural  
1046 catchment, *Agric. Water Manag.*, 92, 171-182, <https://doi.org/10.1016/j.agwat.2007.05.015>,  
1047 2007.

1048

1049 Macrae, M. L., Ali, G. A., King, K. W., Plach, J. M., Puer, W. T., Williams, M., Morison, M.  
1050 Q., and Tang, W.: Evaluating Hydrologic Response in Tile-Drained Landscapes: Implications for  
1051 Phosphorus Transport, *J. Environ. Qual.*, 48(5), 1347-1355,  
1052 <https://doi.org/10.2134/jeq2019.02.0060>, 2019.

1053

1054 Malzone, J. M., Lowry, C. S., and Ward, A. S.: Response of the hyporheic zone to transient  
1055 groundwater fluctuations on the annual and storm event time scales, *Water Resour. Res.*, 52,  
1056 5301-5321, <https://doi.org/10.1002/2015WR018056>, 2016.

1057

1058 [Mizukami, N., Clark, M. P., Sampson, K., Nijssen, B., Mao, Y., McMillan, H., Viger, R. J.,](#)  
1059 [Markstrom, S. L., Hay, L. E., Woods, R., Arnold, J. R., & Brekke, L. D. \(2016\). mizuRoute](#)  
1060 [version 1: A river network routing tool for a continental domain water resources applications.](#)  
1061 [Geoscientific Model Development, 9, 2223–2238. <https://doi.org/10.5194/gmd-9-2223-2016>](#)  
1062 Moriasi, D. N., Arnold, J. G., Van Liew, M. W., Bingner, R. L., Harmel, R. D., and Veith, T. L.:  
1063 Model Evaluation Guidelines for Systematic Quantification of Accuracy in Watershed  
1064 Simulations, Trans. ASABE, 50(3), 885-900, <https://doi.org/10.13031/2013.23153>, 2007.  
1065  
1066 Moriasi, D. N., Gowda, P. H., Arnold, J. G., Mulla, D. J., Ale, S., Steiner, J. L., and Tomer, M.  
1067 D.: Evaluation of the Hooghoudt and Kirkham Tile Drain Equations in the Soil and Water  
1068 Assessment Tool to Simulate Tile Flow and Nitrate-Nitrogen, J. Environ. Qual., 42, 1699-1710,  
1069 <https://doi.org/10.2134/jeq2013.01.0018>, 2013.  
1070  
1071 Plach, J. M., Macrae, M. L., Ali, G. A., Brunke, R. R., English, M. C., Ferguson, G., Lam, W.  
1072 V., Lozier, T. M., McKague, K., O’Halloran, I. P., Opolko, G., and Van Esbroeck, C. J.: Supply  
1073 and Transport Limitations on Phosphorus Losses from Agricultural Fields in the Lower Great  
1074 Lakes Region, Canada, J. Environ. Qual., 47, 96-105, <https://doi.org/10.2134/jeq2017.06.0234>,  
1075 2018a.  
1076  
1077 Plach, J. M., Macrae, M. L., Williams, M. R., Lee, B. D., and King, K. W.: Dominant glacial  
1078 landforms of the lower Great Lakes region exhibit different soil phosphorus chemistry and  
1079 potential risk for phosphorus loss, J. Great Lakes Res., 44, 1057-1067,  
1080 <https://doi.org/10.1016/j.jglr.2018.07.005>, 2018b.

1081

1082 Plach, J., Pluer, W., Macrae, M., Kompanizare, M., McKague, K., Carlow, R., and Brunke, R.:

1083 Agricultural Edge of Field Phosphorus Losses in Ontario, Canada: Importance of the

1084 Nongrowing Season in Cold Regions, *J. Environ. Qual.*, 48, 813-821,

1085 <https://doi.org/10.2134/jeq2018.11.0418>, 2019.

1086

1087 Pluer, W. T., Macrae, M., Buckley, A., and Reid, K.: Contribution of preferential flow to tile

1088 drainage varies spatially and temporally, *Vadose Zone J.*, 19: e20043,

1089 <https://doi.org/10.1002/vzj2.20043>, 2020.

1090

1091 Pomeroy, J. W., Gray, D. M., Shook, K. R., Toth, B., Essery, R. L. H., Pietroniro, A., and

1092 Hedstrom, N. R.: An evaluation of snow accumulation and ablation processes for land surface

1093 modelling, *Hydrol. Process.*, 12, 2339-2367, [https://doi.org/10.1002/\(SICI\)1099-](https://doi.org/10.1002/(SICI)1099-1085(199812)12:15)

1094 [1085\(199812\)12:15](https://doi.org/10.1002/(SICI)1099-1085(199812)12:15), 1998.

1095

1096 Pomeroy, J. W., Gray, D. M., Brown, T., Hedstrom, N. R., Quinton, W. L., Granger, R. J., and

1097 Carey, S. K.: The cold regions hydrological model: a platform for basing process representation

1098 and model structure on physical evidence, *Hydrol. Process.*, 21, 2650-2667,

1099 <https://doi.org/10.1002/hyp.6787>, 2007.

1100

1101 Pomeroy, J. W., Fang, X., Shook, K., and Whitfield, P. H.: Predicting in Ungauged Basins Using

1102 Physical Principles Obtained Using the Deductive, Inductive, and Abductive Reasoning

1103 Approach, <https://research->  
1104 [groups.usask.ca/hydrology/documents/pubs/papers/pomeroy\\_et\\_al\\_2003\\_3.pdf](https://research-groups.usask.ca/hydrology/documents/pubs/papers/pomeroy_et_al_2003_3.pdf) , 2013.  
1105  
1106 Pomeroy, J. W., Fang, X., and Marks, D. G.: The cold rain-on-snow event of June 2013 in the  
1107 Canadian Rockies - characteristics and diagnosis, *Hydrol. Process.*, 30, 2899-2914,  
1108 <https://doi.org/10.1002/hyp.10905>, 2016.  
1109  
1110 Pomeroy, J. W., Brown, T., Fang, X., Shook, K. R., Pradhananga, D., Armstrong, R., Harder, P.,  
1111 Marsh, C., Costa, D., Krogh, S. A., Aubry-Wake, C., Annand, H., Lawford, P., He, Z.,  
1112 Kompanizare, M., and Lopez Moreno, J. I.: The cold regions hydrological modelling platform  
1113 for hydrological diagnosis and prediction based on process understanding, *J. of Hydrol.*, 615 (A),  
1114 128711, <https://doi.org/10.1016/j.jhydrol.2022.128711>, 2022.  
1115  
1116 Qi, P., Zhang, G., Xu, Y. J., Wang, L., Ding, C., and Cheng, C.: Assessing the Influence of  
1117 Precipitation on Shallow Groundwater Table Response Using Combination of Singular Value  
1118 Decomposition and Cross-Wavelet Approaches, *Water*, 10, 598,  
1119 <https://doi.org/10.3390/w10050598>, 2018.  
1120  
1121 Quinton, J. G., Govers, G., van Oost, K., and Bardgett, R.: The impact of agricultural soil erosion  
1122 on biochemical cycling, *Nat. Geosci.*, 3, 311-314, <https://doi.org/10.1038/ngeo838>, 2010.  
1123



1124 Raats, P. A. C. and Gardner, W. R.: Movement of water in saturated zone near a water table. Ch.  
1125 13 in Drainage for agriculture, J. van Schilfgraade, Ed., Agronomy Monograph. No. 17,  
1126 American Society of Agronomy, Madison, WI, pp. 331-357, 1974.  
1127  
1128 Radcliffe, D. E., Reid, D. K., Blomback, K., Bolster, C. H., Collick, A. S., Easton, Z. M.,  
1129 Francesconi, W., Fuka, D. R., Johnsson, H., King, K., Larsbo, M., Youssef, M. A., Mulkey, A.  
1130 S., Nelson, N. O., Persson, K., Ramirez-Avila, J. J., Schmieder, F., and Smith, D. R.:  
1131 Applicability of Models to Predict Phosphorus Losses in Drained Fields: A Review, J. Environ.  
1132 Qual., 44, 614-628, <https://doi.org/10.2134/jeq2014.05.0220>, 2015.  
1133  
1134 Rahman, M. M., Lin, Z., Jia, X., Steele, D. D., and DeSutter, T. M.: Impact of subsurface  
1135 drainage on streamflows in Red River of the North basin, J. Hydrol., 511, 474-483,  
1136 <https://doi.org/10.1016/j.jhydrol.2014.01.070>, 2014.  
1137  
1138 Refsgaard, J. C. and Storm, B.: MIKE SHE. In: Singh VP (ed) Computer models of watershed  
1139 hydrology, Highlands Ranch, Water Research Pub, Colorado, 1995.  
1140  
1141 Richards L. A.: Capillary conduction of liquids through porous medium, Physics, 1 (5): 318-333,  
1142 Bibcode:1931Physi...1..318R. <https://doi.org/10.1063/1.1745010>, 1931.  
1143  
1144 Rozemeijer, J. C., Visser, A., Borren, W., Winegram, M., van der Velde, Y., Klein, J., and  
1145 Broers, H. P.: High-frequency monitoring of water fluxes and nutrient loads to assess the effects

1146 of controlled drainage on water storage and nutrient transport, *Hydrol. Earth Syst. Sci.*, 20, 347-  
1147 358, <https://doi.org/10.5194/hess-20-347-2016>, 2016.

1148

1149 Rust, W., Holman, I., Bloomfield, J. Cuthbert, M., and Corstanje, R.: Understanding the potential  
1150 of climate teleconnections to project future groundwater drought, *Hydrol. Earth Syst. Sci.*, 23,  
1151 3233-3245, <https://doi.org/10.5194/hess-23-3233-2019>, 2019.

1152

1153 Ruttenberg, K.: The global phosphorus cycle. In *Biochemistry*, Vol. 8, treatise on geochemistry,  
1154 Schlesinger W (ed) (eds. H. Holland and K. Turekian). Elsevier-Pergamon: Oxford; 585-643,  
1155 2005.

1156

1157 Searcy, J. and Hardison, C. H.: Double –Mass Curves. *Manual of Hydrology: Part 1, General*  
1158 *Surface-Water Techniques*, Geological Survey Water-Supply Paper 1541-B, 1960.

1159

1160 Schindler, D. W.: Recent advances in the understanding and management of eutrophication,  
1161 *Limnol. Oceanogr.*, 51, 356-363, [https://doi.org/10.4319/lo.2006.51.1\\_part\\_2.0356](https://doi.org/10.4319/lo.2006.51.1_part_2.0356), 2006.

1162

1163 Sharpley, A. N., Hedley, M. J., Sibbesen, E., Hillbricht-Ilkowska, A., House, W. A., and  
1164 Ryszkowski, L.: Phosphorus transfer from terrestrial to aquatic ecosystems, In *Phosphorus in the*  
1165 *global environment*, Tiessen H (ed), Scientific Committee on Problems of the Environment  
1166 (SCOPE). John Wiley & Sons Ltd.: Chichester; 171-199, 1995.

1167

1168 Simunek J., van Genuchten M. Th., and Sejna M.: The HYDRUS Software Package for  
1169 Simulating Two- and Three-Dimensional Movement of Water, Heat and Multiple Solutes in  
1170 Variably-Saturated Media, Technical Manual, Version 2.0, PC Progress, Prague, Czech  
1171 Republic, pp. 258, 2011.

1172

1173 Skaggs, R. W.: A water management model for shallow water table soils, University of North  
1174 Carolina, Water Resource Research Institute, Technical Report 134, 1978.

1175

1176 Skaggs, R. W.: Combination surface-subsurface drainage systems for humid regions. J. Irrig.  
1177 Drain. Div., ASCE. 106(IR4), 265-283, 1980a.

1178

1179 Skaggs, R. W.: Drainmod Reference Report, Methods for Design and Evaluation of Drainage-  
1180 Water Management Systems for Soils with High Water Tables, U.S. Department of Agriculture,  
1181 Soil Conservation Service, North Carolina State University, Raleigh, North Carolina, 1980b.

1182

1183 Skaggs, R. W., Wells, L. G., and Ghate, S. R.: Predicted and measured drainable porosities for  
1184 field soils, Trans. ASAE, 21(3), 522-528, [https://uknowledge.uky.edu/bae\\_facpub/199](https://uknowledge.uky.edu/bae_facpub/199), 1978.

1185

1186 Skaggs, R. W., Youssef, M. A., and Chescheir, G. M.: DRAINMOD: Model Use, Calibration,  
1187 and Validation, Trans. ASABE, 55(4), 1509-1522, <https://doi.org/10.13031/2013.42259>, 2012.

1188

1189 Smedema, L. K., Vlotman, W. F., and Rycroft, D.: Modern land Drainage. Planning, design and  
1190 management of agricultural drainage systems, London: Taylor & Francis.  
1191 <https://doi.org/10.1201/9781003>, 2004.  
1192  
1193 Smith, D. R., King, K. W., Johnson, L., Francesconi, W., Richards, P., Baker, D., and Sharpley,  
1194 A. N.: Surface runoff and tile drainage transport of phosphorus in the Midwestern United States,  
1195 J. Environ. Qual., 44, 495-502, <https://doi.org/10.2134/jeq2014.04.0176>, 2015.  
1196  
1197 Tomer, M. D., Meek, D. W., Jaynes, D. B., and Hatfield, J. L.: Evaluation of nitrate nitrogen  
1198 fluxes from a tile-drained watershed in Central Iowa, J. Environ. Qual., 32, 642-653,  
1199 <https://doi.org/10.2134/jeq2003.6420>, 2003.  
1200  
1201 Twarakavi, N. K. C., Sakai, M., and Simunek, J.: An objective analysis of the dynamic nature of  
1202 field capacity, Water Resour. Res., 45, W10410, <https://doi.org/10.1029/2009WR007944>, 2009.  
1203  
1204 Van Esbroeck, C. J., Macrae, M. L., Brunke, R. I., and McKague, K.: Annual and seasonal  
1205 phosphorus export in surface runoff and tile drainage from agricultural fields with cold temperate  
1206 climates, J. Great Lakes Res., 42(6), 1271-1280, <https://doi.org/10.1016/j.jglr.2015.12.014>, 2016.  
1207  
1208 Van Esbroeck, C. J., Macrae, M. L., Brunke, R. R., and McKague, K.: Surface and subsurface  
1209 phosphorus export from agricultural fields during peak flow events over the nongrowing season  
1210 in regions with cool, temperate climates, Journal of Soil and Water Conservation, 72(1), 65-76,  
1211 <https://doi:10.2489/jswc.72.1.65> , 2017.

1212

1213 Van Schilfgaarde, J.: Nonsteady flow to drains, In *Drainage for Agriculture*, J. van Schilfgaarde,

1214 ed. American Society of Agronomy, Madison, WI. PP 245-270, 1974.

1215

1216 [Vaughan, P. J., Suarez, D. L., Simunek, J., Corwin, D. L., and Rhoades, J. D.: Role of](#)

1217 [Groundwater Flow in Tile Drain Discharge, J. Environ. Qual., 28, 403-410,](#)

1218 <https://doi.org/10.2134/jeq1999.00472425002800020006x>, 1999.

1219

1220 Vidon, P. and Cuadra, P. E.: Impact of precipitation characteristics on soil hydrology in tile

1221 drained landscapes, *Hydrol. Process.*, 24, 1821-1833, <https://doi.org/10.1002/hyp.7627>, 2010.

1222

1223 Vivekananthan, K.: Environmental and Economic Consequences of Tile Drainage Systems in

1224 Canada, The Canadian Agri-Food Policy Institute, [www.capi-icpa.ca](http://www.capi-icpa.ca), 2019.

1225

1226 Vivekananthan, K., Macrae, M., Lobb, D. A., and Ali, G. A.: Contribution of overland and tile

1227 flow to runoff and nutrient losses from vertisols in Manitoba, Canada, *J. Environ. Qual.*, 48(4),

1228 959-965, <https://doi.org/10.2134/jeq2019.03.0103>, 2019.

1229

1230 Waichler, S. R. and Wigmosta, M. S.: Development of Hourly Meteorological Values from

1231 Daily Data and Significance to Hydrological Modeling at H. J. Andrews Experimental Forest,

1232 *Am. Meteorol. Soc.*, 4, 251-263, [https://doi.org/10.1175/1525-](https://doi.org/10.1175/1525-7541(2003)4<251:DOHMFV>2.0.CO;2)

1233 [7541\(2003\)4<251:DOHMFV>2.0.CO;2](https://doi.org/10.1175/1525-7541(2003)4<251:DOHMFV>2.0.CO;2), 2003.

1234

1235 Williams, M. R., King, K. W., and Fausey, N. R.: Drainage water management effects on tile  
 1236 discharge and water quality, *Agric. Water Manag.*, 148, 43-51,  
 1237 <http://dx.doi.org/10.1016/j.agwat.2014.09.017>, 2015.

1238  
 1239 Williams, M. R., King, K. W., Ford, W., Buda, A. R., and Kennedy, C. D.: Effect of tillage on  
 1240 macropore flow and phosphorus transport to tile drains, *Water Resour. Res.*, 52, 2868-2882,  
 1241 <https://doi.org/10.1002/2015WR017650>, 2016.

1242  
 1243 Williams, M. R., Livingston, S. J., Heathman, G. C., and McAfee, S. J.: Thresholds for run-off  
 1244 generation in a drained closed depression, *Hydrol. Process.*, 1-14,  
 1245 <https://doi.org/10.1002/hyp.13477>, 2019.

1246  
 1247 Youngs, E. G.: Effect of the Capillary fringe on Steady-State Water Tables in drained Lands, *J.*  
 1248 *Irrig. Drain. Eng.*, 138(9), 809-814, [https://doi.org/10.1061/\(ASCE\)IR.1943-4774.0000467](https://doi.org/10.1061/(ASCE)IR.1943-4774.0000467),  
 1249 2012.

1250

1251

1252 **Appendix A**

1253 Table A1. Instrument names and descriptions

Instrument name	Description
Hach Flo-tote and FL900 logger	Flow velocity and water level measurement
U20, Onset Ltd.	Barometrically-corrected pressure transducer
Temperature Smart Sensor S-THB-M002	Air temperature measurement

Wind Smart Sensor S-WSET-M002	Wind speed measurement
(Silicon Pyranometer)-S-LIB-M003	Solar radiation sensor
Tipping bucketrain gauge, 0.2 mm Rainfall Smart Sensor – SRGB-M002	Rainfall measurement
RH Smart Sensor(S-THB-M002)	Relative Humidity measurement

1254

1255

1256

1257 **Appendix B**

1258 Table B1. Parameter names and their symbols in CRHM platform

Parameter symbol	Parameter name
Tair	Air temperature
Wspeed	Wind speed
RH	Relative Humidity
Qsi	Incoming solar irradiance
R	Rainfall
WQ_soil	Water Quality soil module
<u>soil_WL/SWL</u> <u>SWTWT</u>	<u>Soil water</u> <u>Water level</u> <u>table</u> elevation above the semipermeable layer
<u>SSS</u>	<u>Soil saturated storage</u> or the <u>saturated part of the soil moisture</u>
soil_moist	Soil moisture
Porosity_soil	Soil porosity
AL	Above layer
BL	Below layer

GWRD	Groundwater level fluctuations, groundwater recharge and discharge
------	--

1259

1260

1261

1262 **Appendix C**

1263

1264 We show how we assess seasonal factors ( $f_{y,i}$ ) for different years in this study. Equation (4) can  
 1265 be written as:

1266

1267  $G_{y,i} = G \times f_{y,i}$  (C1)

1268

1269 For each year ( $y$ ),  $f_{y,i}$  for the first ( $f_{y,1}$ ) and second ( $f_{y,2}$ ) part of the sine function ( $G$ ), where  
 1270  $G \geq 0$  and  $G < 0$  respectively, were defined as:

1271

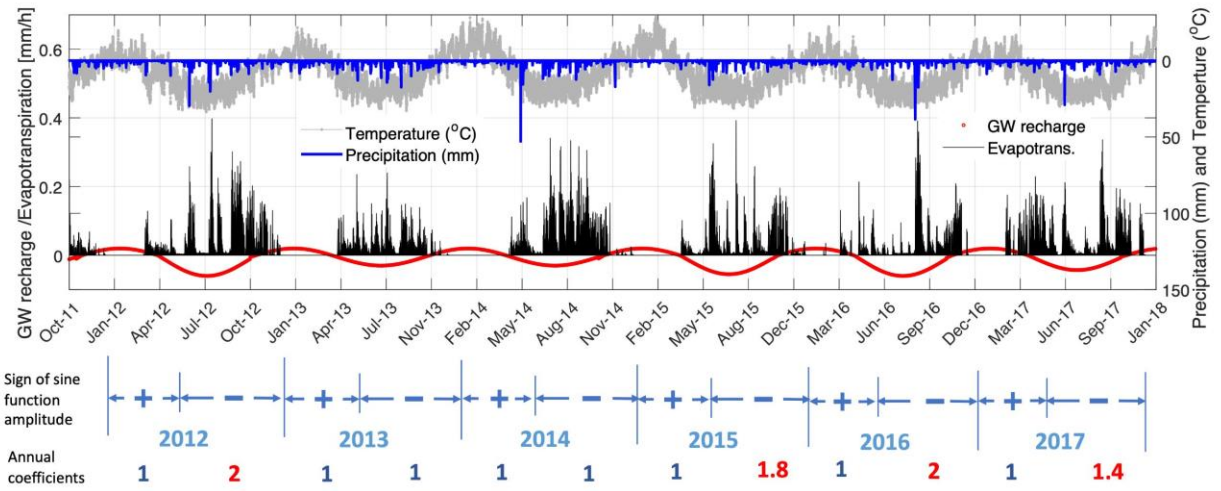
1272 
$$\begin{cases} \text{if } G \geq 0 \text{ [ } i = 1 \text{ ] then } f_{y,1} = x \\ \text{if } G < 0 \text{ [ } i = 2 \text{ ] then } f_{y,2} = y \end{cases}$$
 (C-2)

1273

1274  $G$  is the sine function representing the annual fluctuations in [soil-waterwater leveltable](#)  
 1275 [\(SWTWT/SSS\)](#). So, for  $n$  years there are  $n \times 2$   $f_{y,i}$  values. The default values for  $f_{y,i}$  are 1 and  
 1276 the default values can be changed for each year and for first and second parts in each year  
 1277 independently. Calculated  $G_{y,i}$  in each time step add or subtracted to or from the total soil  
 1278 moisture depend on the its sign. The values for the sine function parameters are in Fig. C1. The  
 1279 verified sine function time series along with time series of temperature, precipitation and



1280 calculated evapotranspiration are shown in Fig. C1. In this figure it is obvious that in years 2012  
 1281 and 2015 to 2017 the warm season amplitudes are larger. The ET values are happenhappened  
 1282 more in the warm seasons (growing seasons). Also, it can be seen that the seasonal oscillation in  
 1283 sine function is very similar to the temperature general oscillations.



1284  
 1285 Figure C1. Time series of the adjustable sine function along with the time series of calculated evapotranspiration, temperature  
 1286 and precipitation during the study period from Oct 2011 to Sept 2018.